

From Bethe-Salpeter Wave Functions to Generalised Parton Distributions

C. Mezrag^{1*}, H. Moutarde^{2†}, J. Rodríguez-Quintero^{3‡}

¹ *Physics Division, Argonne National Laboratory*

Argonne, Illinois 60439, USA

² *CEA, Centre de Saclay, IRFU/Service de Physique Nucléaire*

F-91191 Gif-sur-Yvette, France

³ *Departamento de Física Aplicada, Facultad de Ciencias Experimentales*

Universidad de Huelva, Huelva 21071, Spain.

January 19, 2022

Abstract

We review recent works on the modelling of Generalised Parton Distributions within the Dyson-Schwinger formalism. We highlight how covariant computations, using the impulse approximation, allows one to fulfil most of the theoretical constraints of the GPDs. Specific attention is brought to chiral properties and especially the so-called soft pion theorem, and its link with the Axial-Vector Ward-Takahashi identity. The limitation of the impulse approximation are also explained. Beyond impulse approximation computations are reviewed in the forward case. Finally, we stress the advantages of the overlap of lightcone wave functions, and possible ways to construct covariant GPD models within this framework, in a two-body approximation.

Keywords: Generalised Parton Distributions, Dyson-Schwinger Equations, Double Distributions, PDF, pion

Contents

| | | |
|----------|---|----------|
| 1 | Introduction | 3 |
| 2 | Hadron structure | 4 |
| 2.1 | GPD | 4 |
| 2.1.1 | Definition | 4 |
| 2.1.2 | Support and symmetry properties | 5 |
| 2.1.3 | Forward limit, positivity and polynomiality | 6 |
| 2.1.4 | Exclusive processes and GPD extraction | 8 |
| 2.1.5 | Evolution | 9 |
| 2.1.6 | 3D picture of hadrons | 10 |
| 2.2 | Double Distributions | 10 |
| 2.2.1 | Definition and relation to GPDs | 10 |
| 2.2.2 | Ambiguity and schemes | 11 |
| 2.3 | Phenomenological models in a nutshell | 12 |

*cmezrag@anl.gov

†herve.moutarde@cea.fr

‡jose.rodriguez@dfaie.uhu.es

| | | |
|----------|--|-----------|
| 3 | Dyson-Schwinger equations | 12 |
| 3.1 | Basic equations and truncation schemes | 13 |
| 3.1.1 | The Gap equation | 13 |
| 3.1.2 | The Bethe-Salpeter equation | 14 |
| 3.1.3 | Truncation schemes and symmetries | 15 |
| 3.2 | The Nakanishi representation | 16 |
| 3.2.1 | Interpolating functions | 17 |
| 3.2.2 | An algebraic model | 17 |
| 4 | Covariant computation of the pion GPD | 18 |
| 4.1 | Pion GPD Mellin moments | 18 |
| 4.1.1 | Local Impulse Approximation | 18 |
| 4.1.2 | Computations of Mellin Moments | 19 |
| 4.1.3 | Comparison to available data | 21 |
| 4.2 | From Mellin moments to GPDs | 22 |
| 4.2.1 | Tensorial structure and Double Distributions | 22 |
| 4.2.2 | GPDs reconstruction: successes and weaknesses | 23 |
| 5 | Chiral properties and soft pion theorem | 25 |
| 5.1 | Consequences of the Axial-Vector Ward Takahashi Identity | 25 |
| 5.2 | Soft Pion Theorem | 25 |
| 6 | Beyond the impulse approximation | 28 |
| 6.1 | Forward kinematics implications | 28 |
| 6.1.1 | Asymmetry of the PDF | 28 |
| 6.1.2 | Additional symmetrising Contributions | 28 |
| 6.1.3 | Computations and results | 30 |
| 6.2 | Three-dimensional sketch of the pion | 32 |
| 6.3 | Strength and weakness of the covariant approach | 34 |
| 7 | Lightcone formalism | 35 |
| 7.1 | Lightcone wave functions | 35 |
| 7.1.1 | Basic facts on lightcone formalism | 35 |
| 7.1.2 | Hadrons in the lightcone formalism | 36 |
| 7.1.3 | Pion lightcone and Bethe-Salpeter wave functions | 36 |
| 7.2 | Overlap of pion wave functions | 37 |
| 7.2.1 | GPDs and LCWFs | 37 |
| 7.2.2 | An example with the algebraic model | 39 |
| 7.3 | Overlap and polynomiality | 40 |
| 8 | Conclusion | 41 |
| A | Conventions and Notations | 43 |
| A.1 | Space-time and lightcone conventions | 43 |
| A.2 | Dirac Algebra | 43 |
| A.3 | Euclidean space | 43 |
| A.4 | Gordon Identity | 44 |
| | References | 44 |

1 Introduction

Since they have been introduced in the 1990s, Generalised Parton Distributions [1–3] (GPDs) have been under a strong scientific investigation, both experimentally and theoretically, as testify the number of dedicated review papers [4–9]. Recently, the interest for GPDs have even been increased by the publication of new experimental data [10, 11]. In the near future, the upgrade of the Jefferson Laboratory facility from 6 GeV to 12 GeV should provide the GPD community with very accurate experimental data on a wide kinematic range in the so-called “valence region”. In the kinematic region dominated by sea quarks and gluon contributions, COMPASS in a short time scale [12], and EIC in a longer time scale [13] should also provide brand new experimental data.

On the theoretical side, the GPD framework is now well established. Evolution equations are known up to next-to-leading order, and some of the higher-twist corrections have been implemented successfully up to twist-four [14, 15]. From this situation, several phenomenological models have flourished [16–20], allowing the description of worldwide available experimental data, with a reasonable accuracy. Using those phenomenological models, extraction of GPDs from experiments has been performed, providing a three-dimensional sketch of the nucleon, but still in the limit of the considered approximations, like for instance, computations at leading order in α_s , the strong coupling constant (see *e.g.* Ref. [9]). If few attempts have been made to compute GPDs beyond phenomenological models [21–25], they have not encountered the successes of the latter ones, when compared to experimental data. Nonetheless, it should be emphasised that such a task plays a key role in the ambitious purpose of validating our basic understanding of the strong interactions by the use of GPDs.

As GPDs encode non-perturbative information on hadrons, any model built within a bottom-up approach must be intrinsically non-perturbative. Among the different possible ways, we focus here on the Dyson-Schwinger equations [26–28] (DSEs) and on the Bethe-Salpeter equation [27–31] (BSE). DSEs consist in coupled, self-consistent equations, relating the Green functions of QCD among themselves. The BSE is also a self-consistent equation, coupled to the Green functions of QCD, allowing one to compute the so-called Bethe-Salpeter wave function for a given meson. In the recent years, significant progresses have been made in order to solve consistently these equations in a symmetry-preserving approximation scheme [32]. It is now possible to compute within the DSEs framework, a significant number of observables, like mesons masses and decay constants (see *e.g.* Ref. [33]) or form factors [34] with a reasonable accuracy.

The idea of computing hadron structure within a DSEs-BSE framework is not new, since one can tally different approaches to compute GPDs from DSEs-BSE developed during the last fifteen years [35–39]. Nevertheless, it was not possible at that time to rely on proper symmetry-preserving truncation schemes. This has recently changed with the computation of the pion Distribution Amplitude (DA) [40], paving the way for similar developments on more complex objects, especially on PDFs [41] and GPDs [42, 43].

Giving technical details on GPDs and DSEs would require a large number of pages. *A contrario*, the present work focuses on a specific aim: highlighting progresses made in modelling GPDs in a DSEs framework. Therefore, the reader looking for extended proofs is invited to refer to the original work or to the following reviews Refs. [6, 7] for GPDs and Refs. [44, 45] for DSEs.

The present review is organised as it follows. In section 2 the main properties of GPDs are outlined. In addition, a related object, called Double Distribution (DD) is introduced. Then, in section 3, basic facts on DSEs-BSE are given, including insight of techniques and truncation schemes used to solved the coupled equations. Section 4 highlights the advantages and drawbacks of computing pion GPDs in a covariant framework. Light is also shed on chiral properties of the chiral-even pion GPD in section 5, showing that the rainbow ladder truncation scheme is consistent with the soft pion theorem. Section 6 shows the limitations of the so-called impulse approximation, mainly used in covariant approaches, and the way to go beyond it in the forward case. In section 7, the possibility to compute GPDs using the lightcone formalism is emphasised, and the consequences in terms of DSEs are explored. Finally, the conclusion is given in section 8.

2 Hadron structure

This section is devoted to introduce the definition, basic properties and main features related to GPDs. Then, we pay special attention to the modelling approach based on the so-called double distributions that have the merit to guarantee, by construction, the fulfilling of the main properties resulting from the observation of fundamental symmetries for the GPDs. In further sections, this fulfilling will be, as should be, a cornerstone for the building of a GPD model based on the computational framework provided by DSE and BSE.

2.1 GPD

Starting by the definition of GPDs¹, we discuss then their main properties and features, as their evolution with the factorisation scale or extraction from exclusive processes.

2.1.1 Definition

Formally, GPDs are defined as the Fourier transform of a non-local matrix element. In the case of a spin-1/2 hadron, two GPDs are required to fully parameterise the following matrix element:

$$\begin{aligned} F^q &= \frac{1}{2} \int \frac{dz^-}{2\pi} e^{ixP^+z^-} \langle p_2 | \bar{\psi}^q \left(-\frac{z}{2} \right) \gamma^+ \psi^q \left(\frac{z}{2} \right) | p_1 \rangle \Big|_{z^+=z_\perp=0} \\ &= \frac{1}{2P^+} \left[H^q(x, \xi, t) \bar{u}(p_2) \gamma^+ u(p_1) + E^q(x, \xi, t) \bar{u}(p_2) \frac{i\sigma^{+\mu} \Delta_\mu}{2M} u(p_1) \right], \end{aligned} \quad (1)$$

with ψ^q being the quark field of flavour q , p_1 and p_2 are respectively the momenta of the incoming and outgoing hadron, $P = \frac{p_1+p_2}{2}$ and $\Delta = p_2 - p_1$. The lightcone variables are defined in appendix A. $\xi = -\frac{\Delta^+}{2P^+}$ is called the skewness, t is the Mandelstam variable such that $t = \Delta^2$, and M is the mass of the considered hadron. Working in the lightcone gauge, the Wilson line $[-\frac{z}{2}; \frac{z}{2}]$ reduces to 1 and is thus omitted here. Additional quark GPDs can be defined through:

$$\begin{aligned} \tilde{F}^q &= \frac{1}{2} \int \frac{dz^-}{2\pi} e^{ixP^+z^-} \langle p_2 | \bar{\psi}^q \left(-\frac{z}{2} \right) \gamma^+ \gamma_5 \psi^q \left(\frac{z}{2} \right) | p_1 \rangle \Big|_{z^+=z_\perp=0} \\ &= \frac{1}{2P^+} \left[\tilde{H}^q(x, \xi, t) \bar{u}(p_2) \gamma^+ \gamma_5 u(p_1) + \tilde{E}^q(x, \xi, t) \bar{u}(p_2) \frac{\gamma_5 \Delta^+}{2M} u(p_1) \right], \end{aligned} \quad (2)$$

as well as gluon GPDs:

$$\begin{aligned} F^g &= \frac{1}{P^+} \int \frac{dz^-}{2\pi} e^{ixP^+z^-} \langle p_2 | G^{+\mu} \left(-\frac{z}{2} \right) G_\mu^+ \left(\frac{z}{2} \right) | p_1 \rangle \Big|_{z^+=z_\perp=0} \\ &= \frac{1}{2P^+} \left[H^g(x, \xi, t) \bar{u}(p_2) \gamma^+ u(p_1) + E^g(x, \xi, t) \bar{u}(p_2) \frac{i\sigma^{+\mu} \Delta_\mu}{2M} u(p_1) \right], \end{aligned} \quad (3)$$

$$\begin{aligned} \tilde{F}^g &= \frac{1}{2} \int \frac{dz^-}{2\pi} e^{ixP^+z^-} \langle p_2 | G^{+\mu} \left(-\frac{z}{2} \right) \tilde{G}_\mu^+ \left(\frac{z}{2} \right) | p_1 \rangle \Big|_{z^+=z_\perp=0} \\ &= \frac{1}{2P^+} \left[\tilde{H}^g(x, \xi, t) \bar{u}(p_2) \gamma^+ \gamma_5 u(p_1) + \tilde{E}^g(x, \xi, t) \bar{u}(p_2) \frac{\gamma_5 \Delta^+}{2M} u(p_1) \right], \end{aligned} \quad (4)$$

where $G^{\mu\nu}$ is the gluon field strength and $\tilde{G}^{\mu\nu} = \frac{1}{2} \epsilon_{\mu\nu\rho\sigma} G^{\rho\sigma}$. In the case of the pion, which will be our main topic later on, spinlessness and discrete symmetries restrict the parameterisation of these matrix elements to two GPDs:

$$H_\pi^q(x, \xi, t) = \frac{1}{2} \int \frac{dz^-}{2\pi} e^{ixP^+z^-} \langle p_2 | \bar{\psi}^q \left(-\frac{z}{2} \right) \gamma^+ \psi^q \left(\frac{z}{2} \right) | p_1 \rangle \Big|_{z^+=z_\perp=0}, \quad (5)$$

$$H_\pi^g(x, \xi, t) = \frac{1}{P^+} \int \frac{dz^-}{2\pi} e^{ixP^+z^-} \langle p_2 | G^{+\mu} \left(-\frac{z}{2} \right) G_\mu^+ \left(\frac{z}{2} \right) | p_1 \rangle \Big|_{z^+=z_\perp=0}. \quad (6)$$

In the following, unless explicitly said, we will focus on the pion quark GPD H_π^q .

¹We stick on chiral-even GPDs only. Transversity GPDs are described in Ref. [46].

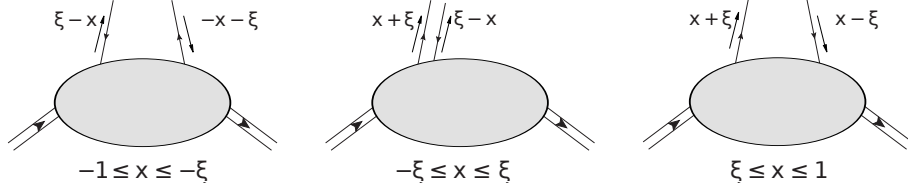


Figure 1: Different interpretations of the GPD. Left-hand side: kinematic corresponding to an antiquark; centre: kinematic corresponding to a quark antiquark pair; right-hand side: kinematic corresponding to a quark.

2.1.2 Support and symmetry properties

From the definition of GPDs in terms of matrix elements, it is possible to derive theoretical properties coming from field theory. First of all, one has to deal with the so-called support properties of the GPDs, stating that:

$$(x, \xi) \in [-1; 1]^2, \quad (7)$$

which can be obtained from amplitude computations [47]. Depending on respective values of x and ξ , one has different possible interpretations of the GPDs as shown on figure 1. The two lines $x = \pm\xi$ play a crucial role. They define the central region, often called ERBL, to the outer one called the DGLAP region. In order to ensure the factorisation of processes between a hard part computed using pQCD and soft parts including GPDs, the latter must be continuous on the lines $x = \pm\xi$ (see section 2.1.4). In addition to x , ξ and t , GPDs also depend on a factorisation scale μ_F , and a renormalisation scale μ_R , usually taken equal. These dependences are omitted for brevity but will be discussed below in this section.

GPDs are also constrained by discrete symmetries. Gluons being their own antiparticles, gluon GPDs H^g and E^g are even in x , whereas \tilde{H}^g and \tilde{E}^g are odd. Quark GPDs generally do not have any symmetry properties with respect to x , but still, combinations can be defined as:

$$\begin{aligned} H^{q(+)}(x, \xi, t) &= H^q(x, \xi, t) - H^q(-x, \xi, t), \\ \tilde{H}^{q(+)}(x, \xi, t) &= \tilde{H}^q(x, \xi, t) + \tilde{H}^q(-x, \xi, t), \end{aligned} \quad (8)$$

and correspond to an exchange of a charge $C = 1$ in the t -channel. These combinations are often called “singlet” and can be extended to E^q and \tilde{E}^q . The complementary combinations, labelled $H^{(-)}$, are called non-singlet and correspond to the exchange of a charge $C = -1$ in the t -channel:

$$\begin{aligned} H^{q(-)}(x, \xi, t) &= H^q(x, \xi, t) + H^q(-x, \xi, t), \\ \tilde{H}^{q(-)}(x, \xi, t) &= \tilde{H}^q(x, \xi, t) - \tilde{H}^q(-x, \xi, t). \end{aligned} \quad (9)$$

Contrary to charge conjugation, time reversal invariance has direct consequences on each GPD. For most of them, it implies that the GPD is even in ξ . This is true for both H^q and E^q :

$$H^q(x, \xi, t) = H^q(x, -\xi, t) \quad , \quad E^q(x, \xi, t) = E^q(x, -\xi, t). \quad (10)$$

The different possible cases are detailed in Ref. [7] with computation guidelines. Hermiticity of the theory is also responsible for an important constraint on GPDs. Indeed, taking the hermitian conjugate of equation (1) leads to:

$$[H(x, \xi, t)]^* = H(x, -\xi, t) \quad , \quad [E(x, \xi, t)]^* = E(x, -\xi, t). \quad (11)$$

Injecting the constraint coming from time reversal invariance of equation (10), one can conclude that GPDs are real. This latter statement is true for any GPD.

Due to isospin symmetry, the pion GPDs have additional symmetry properties. In fact, isovector ($I = 1$) and isoscalar ($I = 0$) GPDs can be defined and related to “quark” GPDs as:

$$H^{I=0}(x, \xi, t) = H_{\pi^\pm}^u(x, \xi, t) + H_{\pi^\pm}^d(x, \xi, t) \quad (12)$$

$$= H_{\pi^0}^u(x, \xi, t) + H_{\pi^0}^d(x, \xi, t), \quad (13)$$

$$H^{I=1}(x, \xi, t) = H_{\pi^+}^u(x, \xi, t) - H_{\pi^+}^d(x, \xi, t) \quad (14)$$

$$= -(H_{\pi^-}^u(x, \xi, t) - H_{\pi^-}^d(x, \xi, t)), \quad (15)$$

$$0 = H_{\pi^0}^u(x, \xi, t) - H_{\pi^0}^d(x, \xi, t). \quad (16)$$

Using the previous symmetry properties, H^u and H^d can be related so that for the π^+ , one gets:

$$H^{I=0} = H^u(x, \xi, t) - H^u(-x, \xi, t), \quad (17)$$

$$H^{I=1} = H^u(x, \xi, t) + H^u(-x, \xi, t). \quad (18)$$

And thus isovector and isoscalar GPDs correspond to non-singlet and singlet GPDs respectively.

It is also possible to highlight the chiral properties of the pion GPD, especially the so-called the soft pion theorem. Defining the pion distribution amplitude (DA) φ_π as:

$$f_\pi \varphi_\pi(u) = \int \frac{dz^-}{2\pi} e^{i(2u-1)P^+z^-/2} \langle \pi, P | \bar{\psi}(-\frac{z}{2}) \gamma \cdot n \gamma_5 \psi(\frac{z}{2}) | 0 \rangle \Big|_{z^+=z_\perp=0}, \quad (19)$$

where f_π stands for the pion decay constant, PCAC and crossing symmetry allow one to relate the pion GPDs to the pion DA in the kinematic limit $t \rightarrow 0$ and $\xi \rightarrow 1$ through [48]:

$$H^{I=0}(x, 1, 0) = 0 \quad \text{and} \quad H^{I=1}(x, 1, 0) = \varphi_\pi\left(\frac{1+x}{2}\right). \quad (20)$$

2.1.3 Forward limit, positivity and polynomiality

In the so-called forward limit, *i.e.* when both ξ and t vanish, the GPD H^q reduces itself to the usual parton distribution function. More precisely:

$$H^q(x, 0, 0) = q(x) \quad \text{for } x \geq 0, \quad (21)$$

$$H^q(x, 0, 0) = -\bar{q}(-x) \quad \text{for } x \leq 0, \quad (22)$$

where $q(x)$ and $\bar{q}(x)$ are respectively the PDF of a quark and antiquark of flavour q .

As it is detailed in section 7, the GPDs can be seen on the lightcone as an overlap of lightcone wave-functions [49]. It leads to an additional theoretical property of the GPDs called the positivity property. Indeed, one can consider the GPD H of a scalar hadron at vanishing t as:

$$H(x, \xi) = \sum_S \langle \Psi_{\text{out}}(x, \xi, S) | \Psi_{\text{in}}(x, \xi, S) \rangle, \quad (23)$$

with $\Psi_{\text{in}}(x, \xi, S)$ being the probability amplitude for the hadron to split in a quark carrying a momentum $(x + \xi)P^+$ along the lightcone, and a spectator denoted S . In the same way, $\Psi_{\text{out}}(x, \xi, S)$ corresponds to the probability amplitude to generate the considered hadron from a spectator S and a quark carrying a momentum $(x - \xi)P^+$ along the lightcone. Then the Cauchy-Schwartz inequality yields [50]:

$$\left| \sum_S \langle \Psi_{\text{out}}(x, \xi, S) | \Psi_{\text{in}}(x, \xi, S) \rangle \right|^2 \leq \sum_S \langle \Psi_{\text{out}}(x, \xi, S) | \Psi_{\text{out}}(x, \xi, S) \rangle \sum_{S'} \langle \Psi_{\text{in}}(x, \xi, S') | \Psi_{\text{in}}(x, \xi, S') \rangle. \quad (24)$$

In terms of GPDs and PDFs, this result can be seen as:

$$H^q(x, \xi) \leq \sqrt{q(x_1)q(x_2)}, \quad (25)$$

where

$$x_1 = \frac{x - \xi}{1 - \xi}, \quad x_2 = \frac{x + \xi}{1 + \xi}. \quad (26)$$

The same kind of inequality can be derived for gluon distributions:

$$H^g(x, \xi) \leq \sqrt{(1 - \xi^2)x_1 x_2 g(x_1)g(x_2)}, \quad (27)$$

as well as for other GPDs (including for non-scalar hadrons) [49, 51, 52] or for the so-called impact parameter space GPDs [53].

Last but not least, the Mellin moments $\mathcal{M}_m(\xi, t)$ of the GPDs, defined as:

$$\mathcal{M}_m^H(\xi, t) = \int_{-1}^1 dx \, x^m H(x, \xi, t) \quad , \quad \mathcal{M}_m^E(\xi, t) = \int_{-1}^1 dx \, x^m E(x, \xi, t) \quad (28)$$

shows interesting properties. First, the Mellin moments computed for $m = 0$ give precisely the contributions of the flavour q to the hadron form factors F_1 and F_2 , *i.e.* :

$$\int_{-1}^1 dx \, H^q(x, \xi, t) = F_1^q(t) \quad , \quad \int_{-1}^1 dx \, E^q(x, \xi, t) = F_2^q(t). \quad (29)$$

Then, the Mellin moments can be related to local matrix elements through:

$$\mathcal{M}_m^H(\xi, t) = \frac{1}{2(P^+)^{m+1}} \langle p_2 | \bar{\psi}^q(0) \gamma^+ (i \overleftrightarrow{\partial}^+)^m \psi^q(0) | p_1 \rangle, \quad (30)$$

for a spinless hadron and:

$$\bar{u}(p_2) \left[\gamma^+ \mathcal{M}_m^H(\xi, t) + \frac{\sigma^{+\nu} \Delta_\nu}{2M} \mathcal{M}_m^E(\xi, t) \right] u(p_1) = \frac{1}{2(P^+)^{m+1}} \langle p_2 | \bar{\psi}^q(0) \gamma^+ (i \overleftrightarrow{\partial}^+)^m \psi^q(0) | p_1 \rangle, \quad (31)$$

for spin one-half hadrons, where $\overleftrightarrow{\partial}^+ = \frac{\overrightarrow{\partial}^+ - \overleftarrow{\partial}^+}{2}$. Equations (30) and (31) are valid in the lightcone gauge, but the generalisation to any gauge is straightforward using the covariant derivative \overleftrightarrow{D} instead of the partial one. They can be also seen in terms of covariant local twist-two operators defined as:

$$O^{\{\mu\mu_1 \dots \mu_m\}} = \bar{\psi} \gamma^{\{\mu} i \overleftrightarrow{\partial}^{\mu_1} \dots i \overleftrightarrow{\partial}^{\mu_m\} \psi \quad (32)$$

where $\{\dots\}$ indicates that the operator is totally symmetric and traceless. Projected on the lightcone, the twist-two operators of equation (32) give the ones of equation (31), as expected from the OPE formalism [1, 54, 55]. Covariance allows one to parameterise the matrix element of the local twist-two operators for a spin-1/2 hadron as:

$$\begin{aligned} \langle p_2 | O^{\{\mu\mu_1 \dots \mu_m\}} | p_1 \rangle &= \bar{u}(p_2) \gamma^{\{\mu} u(p_1) \sum_{i=0}^{\left[\frac{m}{2}\right]} A_{m+1, 2i}^q(t) \left(-\frac{\Delta^{\mu_1}}{2}\right) \dots \left(-\frac{\Delta^{\mu_{2i}}}{2}\right) P^{\mu_{2i+1}} \dots P^{\mu_m\}} \\ &\quad + \bar{u}(p_2) \frac{\sigma^{\{\mu\alpha} \Delta_\alpha}{2M} u(p_1) \sum_{i=0}^{\left[\frac{m}{2}\right]} B_{m+1, 2i}^q(t) \Delta^{\mu_1} \dots \Delta^{\mu_{2i}} P^{\mu_{2i+1}} \dots P^{\mu_m\}} \\ &\quad - \text{mod}(2, m) \bar{u}(p_2) \frac{\Delta^{\{\mu}}{2M} u(p_1) C_{m+1}^q(t) \left(-\frac{\Delta^{\mu_1}}{2}\right) \dots \left(-\frac{\Delta^{\mu_m}}{2}\right). \end{aligned} \quad (33)$$

The even power of Δ is a consequence of time reversal invariance as seen in equation (10). In addition, $[\cdot]$ denotes the floor function and $\text{mod}(2, m)$ vanishes when m is even, and is equal to 1 when m is odd. Projecting equation (33) on the lightcone and using the Gordon identity (see appendix A) to reduce from three Dirac structure to two, one can show that:

$$\int dx x^m H(x, \xi, t) = \sum_{j=0}^{\lfloor \frac{m}{2} \rfloor} \xi^{2j} A_{m+1, 2j}^q(t) + \text{mod}(m, 2) \xi^{m+1} C_{m+1}^q(t), \quad (34)$$

$$\int dx x^m E(x, \xi, t) = \sum_{j=0}^{\lfloor \frac{m}{2} \rfloor} \xi^{2j} B_{m+1, 2j}^q(t) - \text{mod}(m, 2) \xi^{m+1} C_{m+1}^q(t). \quad (35)$$

Therefore, the Mellin moments of GPDs are polynomials in ξ . A^q , B^q and C^q are sometimes called generalised form factors in relation with equation (29).

2.1.4 Exclusive processes and GPD extraction

GPDs play a key role in the computation of exclusive processes amplitudes. Therefore, processes like Deeply Virtual Compton Scattering (DVCS), Time-like Compton Scattering (TCS) and Deeply Virtual Meson Production (DVMP) are experimental channels allowing to access GPDs. The amplitudes can be split in a “hard” part, corresponding to the interaction of the active parton with the probe, and a “soft” part, describing non-perturbative phenomena, *i.e.* GPDs and also DAs in the case of DVMP. This is known as the *factorisation theorem* [1, 3, 56–59]. Focusing on DVCS, the total amplitude can be split into four² leading-twist Compton Form Factors (CFF) denoted \mathcal{F} which are related to the chiral-even GPDs through:

$$\mathcal{F}(\xi, t) = \int_{-1}^1 dx C(x, \xi) F(x, \xi, t), \quad (36)$$

where F is the GPD associated with the CFF \mathcal{F} . C corresponds to the coefficient coming from the computation of the perturbative part of the process associated with the GPD \mathcal{F} . The dependencies in terms of the photon virtuality Q^2 , renormalisation and factorisation scales are omitted for brevity. Details will be given in section 2.1.5. In the specific case of the contribution related to the GPD H , with a perturbative coefficient computed at leading order (LO), the associated CFF \mathcal{H} can be written as:

$$\mathcal{H}(\xi, t) = \int_{-1}^1 dx \left(\frac{1}{\xi - x - i\epsilon} - \frac{1}{\xi + x - i\epsilon} \right) H(x, \xi, t). \quad (37)$$

At this point, the continuity of the GPD on the lines $x = \pm\xi$ is required to ensure that the CFF is finite. Still, due to the singularities, the CFF is a complex number, its real and imaginary parts can be computed at LO through:

$$\Re(\mathcal{H}(\xi, t))|_{\text{LO}} = \text{p.v.} \int_{-1}^1 dx \left(\frac{1}{\xi - x} - \frac{1}{\xi + x} \right) H(x, \xi, t), \quad (38)$$

$$\Im(\mathcal{H}(\xi, t))|_{\text{LO}} = \pi (H(\xi, \xi, t) - H(-\xi, \xi, t)), \quad (39)$$

where p.v. is the Cauchy principal value prescription. The imaginary part of this CFF is, for instance, the main contribution to observables depending on beam spin helicities.

Extracting the different CFFs from experimental data reveals itself to be a hard task, partially because few data are available today. In valence region, *i.e.* for large ξ , both Jefferson Laboratory (JLab) Hall A and CLAS collaborations have released DVCS cross-sections [10, 11], as well as asymmetries [60]. In the medium ξ region, the HERMES collaboration has released data for the DVCS asymmetries but not for the cross-sections (see *e.g.* [61]). At low ξ , collider data have

²Twelve when taking into account twist-three and chiral-odd GPDs.

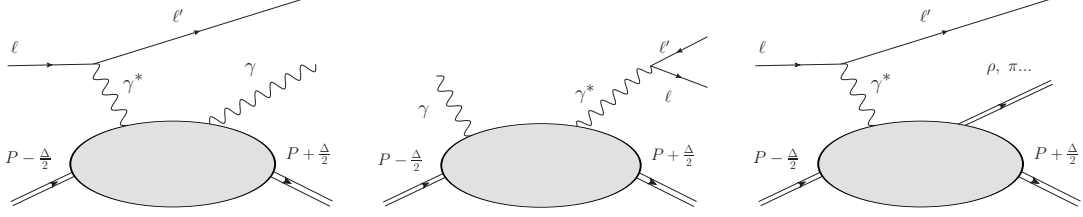


Figure 2: Exclusive processes. Left-hand side: DVCS; center: TCS; right-hand side: DVMP.

been released both by H1 and ZEUS collaborations [62, 63]. Despite this significant experimental effort to measure DVCS observables, a large part of the kinematic domain remains uncovered. Thus several techniques have been developed to extract CFFs, including local fits [64], global fits [19, 65, 66] and extension to neural network are seriously considered today [67].

Interpretations of experimental data are even harder due to the higher order corrections in perturbative QCD, and higher twist corrections. Indeed, if next-to-leading order corrections are well-known for exclusive processes [68–74], it has been shown recently that they have a significant effect on CFFs [75]. In the same way, target mass (*i.e.* higher twist) and finite t corrections [14, 15] are presumably required to fully understand experimental results at intermediate Q^2 [10].

2.1.5 Evolution

Factorisation scale dependence has mainly be omitted until now in this review. Yet, the reader should keep in mind that the splitting of a experimental process between a perturbative part and a non-perturbative object is arbitrary, and that no observable may depend on such a scale. Therefore, from this idea, in the same way than for PDFs, the scale dependence of GPDs can be computed perturbatively. Singlet and non-singlet quark GPDs defined in equations (8) and (9) have different dynamics with respect to evolution. If the former mixes with gluon GPDs, the latter does not. Thus, non-singlet quark GPDs fulfil the following evolution equation:

$$\mu_F^2 \frac{\partial}{\partial \mu_F^2} H^-(x, \xi, t) = \int dy \frac{1}{|\xi|} K_{NS} \left(\frac{x}{\xi}, \frac{y}{\xi} \right) H^-(y, \xi, t), \quad (40)$$

where K_{NS} is the so-called non-singlet evolution kernel. In the singlet case, it is convenient to define the singlet vector \mathbf{H} as:

$$\mathbf{H} = \begin{pmatrix} (2n_f)^{-1} \sum_q H^q(x, \xi, t) - H^q(-x, \xi, t) \\ H^g(x, \xi, t) \end{pmatrix}, \quad (41)$$

where n_f stands for the number of active flavours. \mathbf{H} fulfills a differential equation equivalent to equation (40) using the matrix singlet kernel \mathbf{K} :

$$\mathbf{K} = \begin{pmatrix} K^{qq} \left(\frac{x}{\xi}, \frac{y}{\xi} \right) & K^{qg} \left(\frac{x}{\xi}, \frac{y}{\xi} \right) \\ K^{gq} \left(\frac{x}{\xi}, \frac{y}{\xi} \right) & K^{gg} \left(\frac{x}{\xi}, \frac{y}{\xi} \right) \end{pmatrix}. \quad (42)$$

The evolution kernels K_{NS} and \mathbf{K} can be computed perturbatively and are known at LO [1–3, 76–82] and at NLO [83–87]. As GPDs reduce to PDFs in the forward limit (*i.e.* $\xi \rightarrow 0$), the off-forward evolution kernels K_{NS} and \mathbf{K} also reduce to the non-singlet and singlet DGLAP kernels respectively. While when $\xi \rightarrow 1$, the off-forward evolution kernels reduce to the famous ERBL kernels [88–92] which describe the evolution of DAs. Several techniques have been employed to solve the evolution equations, from numerical approaches [93] or analytic techniques based on the fact that, at LO, the conformal moments diagonalises the evolution equations (see *e.g.* Refs. [6, 7] and references therein for details).

2.1.6 3D picture of hadrons

GPDs present an interesting physical interpretation in the kinematic region $\xi = 0$. For instance, in the case of the pion, the quantity ρ defined as:

$$\rho^q(x, \mathbf{b}_\perp) = \int \frac{d^2\Delta_\perp}{(2\pi)^2} e^{-i\mathbf{b}_\perp \cdot \Delta_\perp} H^q(x, 0, -\Delta_\perp^2), \quad (43)$$

is the probability density to find a quark carrying a momentum fraction x at a given position \mathbf{b}_\perp in the transverse plane [94]. Thus, one gets a *picture* of the pion within a transverse *slice*, perpendicular to the light-cone direction, as can be seen in the example shown in figure 3.

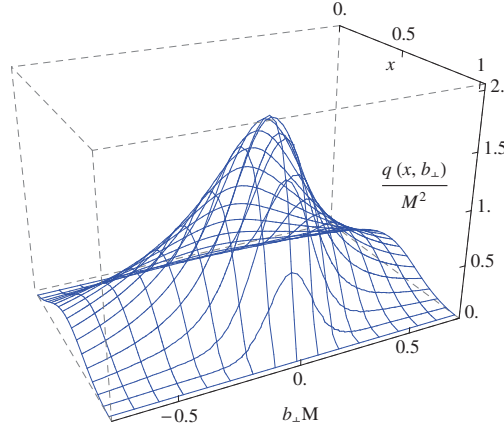


Figure 3: Transverse plane density of the pion GPD H^q . The 3D-plot of $\rho^q(x, \mathbf{b}_\perp)$ comes from Ref. [43]. Acknowledging its rotational invariance, the probability density is only plotted in one of the transverse-plane axes for all x .

2.2 Double Distributions

2.2.1 Definition and relation to GPDs

Originally introduced in [1, 3, 59, 95], Double Distributions (DDs) are an alternative way to encode information contained in non-local matrix elements. In the case of a scalar hadron, two DDs $F^q(\beta, \alpha, t)$ and $G^q(\beta, \alpha, t)$ can be defined as:

$$\begin{aligned} \left\langle P + \frac{\Delta}{2} \left| \bar{q} \left(-\frac{z}{2} \right) \gamma_\mu q \left(\frac{z}{2} \right) \right| P - \frac{\Delta}{2} \right\rangle_{z^2=0} &= 2P_\mu \int_\Omega d\beta d\alpha e^{-i\beta(P \cdot z) + i\alpha \frac{(\Delta \cdot z)}{2}} F^q(\beta, \alpha, t) \\ &\quad - \Delta_\mu \int_\Omega d\beta d\alpha e^{-i\beta(P \cdot z) + i\alpha \frac{(\Delta \cdot z)}{2}} G^q(\beta, \alpha, t) \\ &\quad + \text{higher twist terms.} \end{aligned} \quad (44)$$

The name of the variables follows the conventions of Ref. [5]. β and α have a physical interpretation in terms of parton momenta as shown on figure 4. Discrete symmetries also constrain DDs. For instance, time reversal invariance determines their parity in α : F is even in α whereas G is odd. The DD support, usually denoted Ω , presents a specific rhombus shape:

$$\Omega = \{(\beta, \alpha), |\beta| + |\alpha| \leq 1\}, \quad (45)$$

as shown on figure 4. Being non-perturbative objects, DDs depend on a factorisation scale μ_F and obey to evolution equations [1, 3, 59, 95]. The matrix elements defining GPDs (5) and DDs (44) are very similar, and thus one can show that DDs and GPDs are related through the so-called

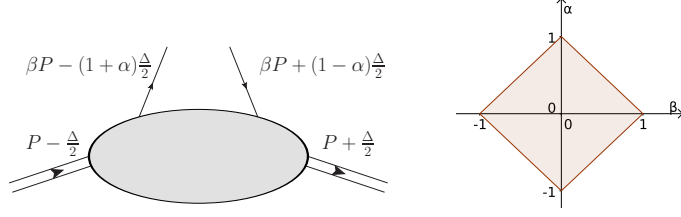


Figure 4: Left-hand side: Momenta associated with hadrons and partons within a DD framework. Right-hand side: DD support.

Radon transform: GPDs are actually the Radon transform of DDs. Practically, one can compute GPDs from DDs through:

$$H^q(x, \xi, t) = \int_{\Omega} d\beta d\alpha (F^q(\beta, \alpha, t) + \xi G^q(\beta, \alpha, t)) \delta(x - \beta - \alpha\xi). \quad (46)$$

Inverting the Radon transform is not an easy task, and thus DD are scarcely computed from GPDs. The polynomiality property can be seen as a direct consequence of equation (46). Computing the Mellin Moment $\mathcal{M}_m(\xi, t)$ in terms of DD leads to:

$$\mathcal{M}_m(\xi, t) = \int_{\Omega} d\beta d\alpha (\beta + \xi\alpha)^m (F^q(\beta, \alpha, t) + \xi G^q(\beta, \alpha, t)), \quad (47)$$

which is a polynomial in ξ of degree at most $m + 1$.

2.2.2 Ambiguity and schemes

Historically, the DD $G^q(\beta, \alpha, t)$ has been overlooked, and introduced only latter in Ref. [21] as the so-called D -term $G^q(\beta, \alpha, t) = \delta(\beta)D(\alpha, t)$. In fact, as shown in Ref. [96] for DDs vanishing on the edges of the rhombus Ω , this D -term corresponds to a *specific scheme* of DD. Indeed, projecting the matrix element of equation (44) on a light-like vector z^μ , it yields:

$$\left\langle P + \frac{\Delta}{2} \left| \bar{q} \left(-\frac{z}{2} \right) z \cdot \gamma q \left(\frac{z}{2} \right) \right| P - \frac{\Delta}{2} \right\rangle_{z^2=0} = -2i \int_{\Omega} d\beta d\alpha e^{-i\beta(Pz) + i\alpha\frac{(\Delta z)}{2}} N^q(\beta, \alpha, t) \quad (48)$$

with

$$N^q(\beta, \alpha, t) = \frac{\partial F^q}{\partial \beta}(\beta, \alpha, t) + \frac{\partial G^q}{\partial \alpha}(\beta, \alpha, t). \quad (49)$$

Therefore, any function σ such that:

$$\sigma^q(\beta, -\alpha, t) = -\sigma^q(\beta, \alpha, t). \quad (50)$$

can be used to modify the DDs $F^q(\beta, \alpha, t)$ and $G^q(\beta, \alpha, t)$:

$$F^q(\beta, \alpha, t) \rightarrow F^q(\beta, \alpha, t) + \frac{\partial \sigma^q}{\partial \alpha}(\beta, \alpha, t), \quad (51)$$

$$G^q(\beta, \alpha, t) \rightarrow G^q(\beta, \alpha, t) - \frac{\partial \sigma^q}{\partial \beta}(\beta, \alpha, t). \quad (52)$$

These transformations leave the effective DD $N^q(\beta, \alpha, t)$ unchanged³. Therefore, both $F^q(\beta, \alpha, t)$ and $G^q(\beta, \alpha, t)$ are not uniquely defined. This has been generalised in Ref. [97] for DD not vanishing on the rhombus edges. Different DD schemes have been used, among them the so-called DD+D,

³It is sometimes called the DD “gauge transformation” due to the possible analogy with electromagnetism [96].

which is the original scheme of Ref. [21], and the one-component DD scheme 1CDD. In the DD+D scheme, $F^q(\beta, \alpha, t)$ and $G^q(\beta, \alpha, t)$ are given by:

$$F^q(\beta, \alpha, t) \rightarrow F_{\text{DD}+\text{D}}^q(\beta, \alpha, t), \quad (53)$$

$$G^q(\beta, \alpha, t) \rightarrow D(\alpha, t)\delta(\beta). \quad (54)$$

Therefore, all the information carried by the variable β is contained in the DD F . The 1CDD scheme introduced in Ref. [98] proceeds from an opposite philosophy as:

$$F_{\text{1CDD}}^q(\beta, \alpha) = \beta f^q(\beta, \alpha), \quad (55)$$

$$G_{\text{1CDD}}^q(\beta, \alpha) = \alpha f^q(\beta, \alpha), \quad (56)$$

and thus the information content is somehow balanced between the two DDs.

2.3 Phenomenological models in a nutshell

Many different phenomenological models of GPDs have been elaborated so far. To close this section, since phenomenology is not the core of the present work, only a brief –surely not exhaustive– enumeration of available phenomenological models will be given in the following. More details can be found for instance in Ref. [9].

Double Distributions have been widely used to build phenomenological models, for they are a simple way to ensure the polynomiality property of GPDs as shown in equation (47). The main available models are the so-called “Goloskokov-Kroll” model [17, 99, 100], modifications of it [101], and the Guidal-Guichon-Vanderhaeghen model [5, 16, 102–104]. Agreement with available experimental data is satisfying [105] but may be challenged by the forthcoming experiments. The so-called dual model [18, 48, 106] consists in expanding the GPDs on Gegenbauer polynomials in the t -channel, and then modeling the coefficients. It has been shown recently [107] that this approach is equivalent to another one, called the Mellin-Barnes model [19, 108]. The latter consists in modeling the conformal moments of a GPD, and then use the Mellin-Barnes inverse transform to compute the GPD itself. Models relying on the Mellin-Barnes parameterisation are in good agreement with available data. Another approach relying on a spectator reggeized diquark model [20] has also been compared to experimental data.

Other approaches have also been developed to model the pion GPD. Polyakov and Weiss [21], and Anikin *et al.* [22], discussed the effect of an instanton vacuum by means of a effective nonlocal quark-hadron lagrangian. Chiral symmetry is also central in the developments of Broniowski *et al.* [23, 24] in the framework of the Nambu-Jona-Lasinio model (see the reviews Ref. [109, 110] and references therein). Choi *et al.* [111, 112], then Mukherjee and Radyushkin [113], proposed light-front calculations with gaussian or power-law wavefunctions in a triangle diagram approximation. Furthermore, GPD modeling in the Bethe-Salpeter framework has enjoyed several studies [35–39], usually with simple Bethe-Salpeter vertices and with computations of triangle diagrams. GPD modeling for large, or moderately large, t , was investigated by Bakulev *et al.* [114], Vogt [115] and Hoodboy *et al.* [116]. Amrath *et al.* [117] modeled the GPD H in the framework of the popular Radyushkin Double Distribution Ansatz [118] and discussed the experimental access to pion GPDs through DVCS on a virtual pion target. At last, let us mention the computation of the generalized form factor in chiral perturbation theory at one-loop order by Diehl *et al.* [119], although only focusses on applications to lattice QCD and does not proceed further to a complete model of the pion GPD.

3 Dyson-Schwinger equations

As mentioned above, our main goal is to pave the way for the building of a GPD model within a framework which relies as much as possible on QCD. This way, we are willing to understand how the dynamical features of the strong interaction generate the structure of hadrons. The framework we will focus on is based on the DSEs and BSEs. The computational scheme relies on

the extraction from QCD equations of motion, namely the DSEs, of the basic ingredients required for obtaining the GPDs within different approaches. Moreover, as one deals with the structure of bound-states formed by quarks, their amplitudes derived from BSEs are also required. Both, DSEs and BSEs are a tower of self-consistent non-perturbative integral equations which should be properly and consistently solved by invoking a particular truncation scheme.

One must also keep in mind that Dyson-Schwinger equations are solved in Euclidean space. Therefore the question of going from Euclidean space to Minkowskian space must be raised. In the following, unless stated otherwise, Euclidean time will be used for computations, *i.e.* Schwinger functions are considered instead of Green functions. We also assume that the measure fulfils the good properties, so that it is possible to get Wightman and Green functions by analytic continuation [120–122]. Therefore, comparison with experimental data will be done in Minkowskian space after analytic continuation of the Schwinger functions.

3.1 Basic equations and truncation schemes

The significant progresses achieved in the last two decades in describing observable properties of hadrons from continuum-QCD [45, 123, 124] are partly due to the application of symmetry-preserving truncation schemes to QCD's DSE [125–128]. The basics of a consistent and symmetry-preserving scheme for DSE and BSE will be briefly discussed below. The first ingredient needed to compute hadron properties from QCD's DSEs is the quark propagator that is to be obtained from the so-called Gap equation.

3.1.1 The Gap equation

The Gap equation relates the quark propagator $S_q(p)$ with the gluon propagator $D^{\mu\nu}(p)$ and the quark-gluon vertex $\Gamma_q^\mu(k, p)$ through:

$$S_q^{-1}(p) = Z_2(i\gamma \cdot p + m_q^0) + Z_1 \int_{\Lambda} \frac{d^4k}{(2\pi)^4} g^2 D_{\mu\nu}(p-k) \gamma^\mu \frac{\lambda^a}{2} S_q(k) \frac{\lambda_a}{2} \Gamma_q^\nu(k, p), \quad (57)$$

where m_q^0 is the considered bare current quark mass and Λ signals that the present integral is well-regularised (this is practically achieved through Pauly-Villars techniques see *e.g.* Ref. [129]). λ^a are the Gell-Mann matrices. In spite of the omission of the renormalisation scale μ_R in equation (57), the reader should keep in mind that the Green functions depend on μ_R , and so do $Z_1(\mu_R, \Lambda)$ and $Z_2(\mu_R, \Lambda)$ which are respectively the quark-gluon vertex and the quark wave function renormalisation constants. Thus the Gap equation is well-defined only when a renormalisation condition is given. This condition is usually taken as:

$$S_q^{-1}(p) \Big|_{p^2=\mu_R^2} = i\gamma \cdot p + m_q(\mu_R^2), \quad (58)$$

with p deeply spacelike. The renormalised current quark mass $m_q(\mu_R^2)$ is related to m_q^0 through:

$$m_q(\mu_R^2) = Z_m^{-1} Z_2 m_q^0, \quad (59)$$

Z_m being the renormalisation constant associated with the Lagrangian mass term. At very large values of μ_R , one expects to recover the bare quark mass. The solution of the Gap equation can be written as:

$$S_q(p) = -i\gamma \cdot p \sigma_{Vq}(p^2, \mu_R^2) + \sigma_{Sq}(p^2, \mu_R^2) = (i\gamma \cdot p A_q(p^2, \mu_R^2) + B_q(p^2, \mu_R^2))^{-1}. \quad (60)$$

Within those notations, when assuming multiplicative renormalisability, it is possible to define the dressed running quark mass $M_q(p^2)$ as:

$$M_q(p^2) = \frac{B_q(p^2, \mu_R^2)}{A_q(p^2, \mu_R^2)}, \quad (61)$$

which does not depend on the renormalisation scale. The dressed quark mass and the renormalised current quark mass are related one to each other through the renormalisation condition (58):

$$m_q(\mu_R^2) = M_q(\mu_R^2). \quad (62)$$

Computation of the dressed quark mass have been performed in the DSE formalism and are in very good agreement with lattice QCD predictions. As shown on figure 5, most of the mass comes from dynamical processes at low energy. This phenomenon is emphasised in the chiral limit, where the entire mass is dynamically generated, and this suggests that DCSB is the origin for most of the visible mass of the Universe.

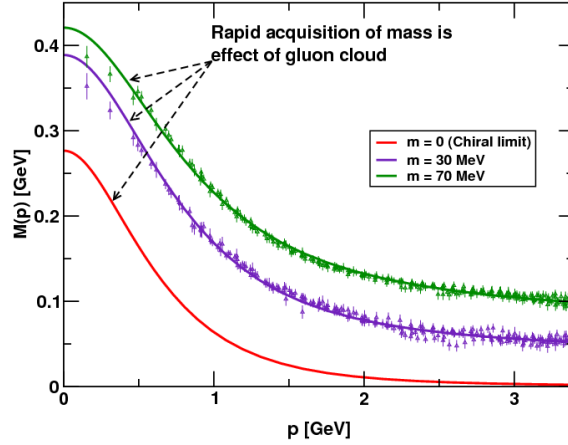


Figure 5: Computations of the dressed quark mass M_q with respect to the quark momentum p within the Dyson-Schwinger equation framework compared to lattice-QCD results. The colours correspond to different bare quark masses. At low p , QCD dynamics generates a significant mass term, even in the chiral limit. Dyson-Schwinger results come from Refs. [130, 131] whereas lattice data are taken from Ref. [132]. This figure comes from Ref. [123].

3.1.2 The Bethe-Salpeter equation

Beyond the quark propagators, as said above, the dynamics of bound states is also studied through non-perturbative objects. Focusing on the pion case, the so-called Bethe-Salpeter wave function $\chi(x_1, x_2)$ [27–31] provides a relativistic description of the bound state in terms of effective quarks and antiquarks,

$$\chi(x_1, x_2) = \langle 0 | T [\psi(x_1) \bar{\psi}(x_2)] | \pi, K \rangle \quad (63)$$

where, for the sake of simplicity, flavour and Dirac indices have been omitted. Owing to translational invariance, it only depends on $x_2 - x_1$ and, in momentum space, reads:

$$\chi(k, K) = \delta(K - k_1 - k_2) \int d^4x e^{ik \cdot x} \langle 0 | T [\psi(\eta x) \bar{\psi}(-(1 - \eta)x)] | \pi, K \rangle \quad (64)$$

with $x = x_2 - x_1$ and

$$\begin{aligned} K &= k_1 + k_2 \\ k &= (1 - \eta)k_1 - \eta k_2 \end{aligned} \quad (65)$$

The pion Bethe-Salpeter amplitude $\Gamma_\pi(p, P)$, related to the Bethe-Salpeter wave function through:

$$\Gamma_\pi(k, K) = S^{-1}(-k_2) \chi(k, K) S^{-1}(k_1), \quad (66)$$

is the solution of the homogeneous Bethe-Salpeter equation:

$$\Gamma_{\pi;ij}(p, P) = \int \frac{d^4k}{(2\pi)^4} [S(k_\eta) \Gamma_\pi(k, P) S(k_\eta)]_{ab} K_{ij}^{ab}(k, p, P), \quad (67)$$

where:

$$\begin{aligned} k_\eta &= k_1 = k + \eta P, \\ k_{\bar{\eta}} &= -k_2 = k - (1 - \eta)P, \end{aligned} \quad (68)$$

and $K_{ij}^{ab}(k, p, P)$ is the quark-antiquark scattering kernel. As the choice of the value of $\eta \in [0, 1]$ is arbitrary, no observable should depend on it. In the case of the pion, the solution of equation (67) is usually projected on a Dirac basis through [133]:

$$\Gamma_\pi(p, P) = \gamma_5 [iE(p, P) + \gamma \cdot P F(p, P) + p \cdot P p \cdot \gamma G(p, P) + \sigma_{\mu\nu} p^\mu P^\nu H(p, P)]. \quad (69)$$

The normalisation of the Bethe-Salpeter amplitude can be derived in a covariant way as [134, 135]:

$$\begin{aligned} 2P^\mu &= \text{Tr}_{\text{CDF}} \left[\int \frac{d^4 k}{2\pi^4} \bar{\Gamma}_\pi(k, P) \frac{\partial S(k_\eta)}{\partial P_\mu} \Gamma_\pi(k, P) S(k_{\bar{\eta}}) \right] \\ &+ \text{Tr}_{\text{CDF}} \left[\int \frac{d^4 k}{2\pi^4} \bar{\Gamma}_\pi(k, P) S(k_\eta) \Gamma_\pi(k, P) \frac{\partial S(k_{\bar{\eta}})}{\partial P_\mu} \right] \\ &+ \text{Tr}_{\text{CDF}} \left[\int \frac{d^4 k}{2\pi^4} \frac{d^4 q}{2\pi^4} \bar{\chi}_\pi(q, P) \frac{\partial K(q, k, P)}{\partial P^\mu} \chi_\pi(k, P) \right] \end{aligned} \quad (70)$$

Tr_{CDF} denoting the trace on colour, Dirac, and flavour indices.

In principle, injecting equation (69) in equation (67) provides a systems of coupled equations. Yet, solving it requires the knowledge of both the fully dressed quark propagator $S_q(p)$, which can be computed from the gap equation (57), and the kernel $K_{ij}^{ab}(k, p, P)$, the exact expression of which remains unknown. Therefore, approximations have to be introduced.

3.1.3 Truncation schemes and symmetries

The main idea is to solve consistently the Bethe-Salpeter and Gap equations. To do so, truncation schemes have been developed. Any truncation scheme needs to be consistent with the fact that the pion is both a QCD bound state and a Goldstone mode of chiral symmetry breaking. So any of them should therefore respects the underlying symmetries and the way some of them are broken. For instance, chiral symmetry is explicitly broken in the so-called Axial-Vector Ward-Takahashi Identity (AVWTI), relating the axial vector vertex $\Gamma_{5\mu}^j(p, P)$ with the pseudoscalar vertex $\Gamma_5^j(p, P)$ through:

$$P^\mu \Gamma_{5\mu}^j(p, P) = \frac{\tau^j}{2} (S^{-1}(k_\eta) i\gamma_5 + i\gamma_5 S^{-1}(k_{\bar{\eta}})) - i[m_{q_1}(\mu_R) + m_{q_2}(\mu_R)] \Gamma_5^j(p, P), \quad (71)$$

the m_q being the renormalised current quark masses, and j indexing the isospin components. Any truncation procedure should be consistent with equation (71).

A possible strategy consists in solving the Bethe-Salpeter equation for the pseudoscalar and axial-vector vertices, and then getting the pion Bethe-Salpeter amplitude as a pole contribution of the two previous ones [136]. Indeed, both $\Gamma_{5\mu}^i(p, P)$ and $\Gamma_5^i(p, P)$ fulfil inhomogenous Bethe-Salpeter equations. For instance in the case of the axial-vector vertex, one gets [137]:

$$\begin{aligned} \Gamma_{5\mu}(p, P) &= Z_2 \gamma_\mu \gamma_5 - Z_1 g^2 \int \frac{d^4 k}{(2\pi)^4} D_{\alpha\beta}(p - k) \frac{\lambda^a}{2} \gamma^\alpha S(-k_{\bar{\eta}}) \Gamma_{5\mu}(k, P) S(k_\eta) \frac{\lambda_a}{2} \Gamma^\beta(q_{\bar{\eta}}, k_{\bar{\eta}}) \\ &+ Z_1 g^2 \int \frac{d^4 k}{(2\pi)^4} D_{\alpha\beta}(p - k) \frac{\lambda^a}{2} \gamma^\alpha S(k_\eta) \frac{\lambda_a}{2} \Lambda_{5\mu\beta}(k, q, P). \end{aligned} \quad (72)$$

This equation is illustrated on figure 6. A similar equation can be derived in the case of the pseudoscalar vertex. Truncation schemes has been developed [32, 125, 126] in order to solve these equations consistently with the AVWTI (71). Two main approximations are usually made to solve

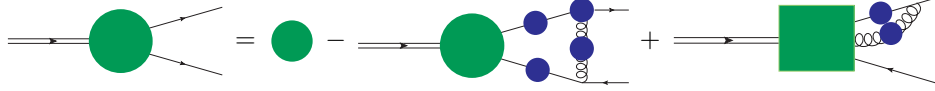


Figure 6: Graphical representation of the inhomogeneous Bethe-Salpeter equation for the axial-vector vertex. The blue circles indicate that the considered Green functions are dressed. The large green circles correspond to $\Gamma_{5\mu}$, the green colour encoding the fact that this object obeys to an inhomogeneous Bethe-Salpeter equation. The small green circle is the inhomogeneous term $\gamma^\mu \gamma_5$, and the green square $\Lambda_{5\mu\nu}$. This graphical representation also works for the pseudoscalar vertex.

the Dyson-Schwinger equations [138]. The first one, called Rainbow Ladder (RL), consists in approximating the kernel of the gap equation as:

$$Z_1 g^2 D_{\mu\nu}(p-k) \Gamma_a^\nu(k, p) = (p-k)^2 \mathcal{G}((p-k)^2) D_{\mu\nu}^{\text{free}}(p-k) \gamma^\nu. \quad (73)$$

In this approach, the free gluon propagator in the Landau gauge $D_{\mu\nu}^{\text{free}}(p-k)$ is dressed by a specific function $\mathcal{G}((p-k)^2)$ reproducing the asymptotic behaviour (see *e.g.* Refs. [127, 136, 139]), and the quark-gluon vertex is taken bare. This choice for the Gap equation kernel is compatible with a choice of $\Lambda_{5\mu\beta} = 0$ in equation (72). Another truncation scheme has been recently developed to improve RL by incorporating the capacity to account non-perturbatively for dynamical chiral symmetry breaking (DCSB) in the integral equations connected with bound-states and is usually described as DB truncation [32]. Therein, the quark-gluon vertex is modelled by using the Ball-Chiu Ansatz (BC) [140] and an additional component generating an Anomalous Chromomagnetic Moment (ACM) [138]:

$$Z_1 g^2 D_{\mu\nu}(p-k) \Gamma_a^\nu(k, p) = \mathcal{G}((p-k)^2) D_{\mu\nu}^{\text{free}}(p-k) Z_2 \tilde{\Gamma}^\nu(k, p), \quad (74)$$

with

$$\tilde{\Gamma}^\nu(k, p) = \Gamma_{\text{BC}}^\nu(k, p) + \Gamma_{\text{ACM}}^\nu(k, p). \quad (75)$$

In this case, the contribution of $\Lambda_{5\mu\beta}$ cannot be ignored anymore. Indeed, DB truncation has been proven to be phenomenologically successful not only describing ground-state vector- and isospin-nonzero pseudoscalar-mesons constituted by light quarks, as RL, but in all the channels considered thus far [33, 40, 128, 141]. It is worth anyhow to remark that the DB kernel for the quark Gap equation has been very recently proved to coincide with the equivalent kernel directly inferred from the analysis of gauge-sector (gluon and ghost propagators) Gap equations [142], namely from an *ab-initio* analysis.

One should keep in mind that Green functions are quantities which remain gauge-dependent, and thus, the presentation below would be incomplete without a word on the choice of the gauge. Usually, the Landau gauge is chosen for multiple reasons. Among them, the Landau gauge is a fixed point of the renormalisation of the covariant gauge parameter. Then it is also the gauge which is the less sensitive to the chosen Ansatz for the quark-gluon vertex as emphasised in Ref. [143, 144]. Finally, it is also the gauge used in lattice computations.

3.2 The Nakanishi representation

Due to the decomposition of equations (60) and (69), solving the Dyson-Schwinger equations consists in computing five scalar functions parameterising the quark propagator and the pion Bethe-Salpeter amplitude (H_π is usually neglected [40]). This is possible numerically, at the cost of discrete momentum variables. Thus one can expect to get numerical grids of functions with a given number of points in p^2 . Even if performing such a computation is already a success, such grids may nevertheless be inadequate to compute other non-perturbative functions. Therefore, interpolating functions have been introduced and successfully fitted on the numerical results here presented.

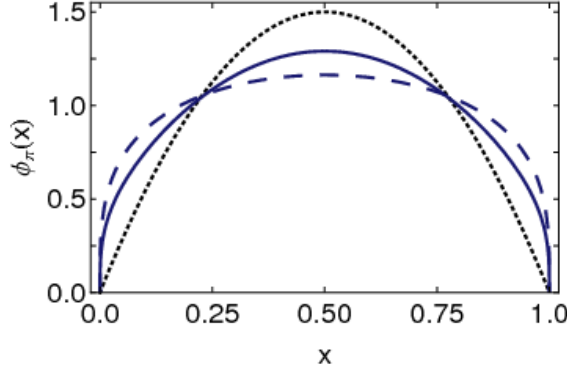


Figure 7: Pion DA computed at renormalisation scale $\mu_R = 2$ GeV. The dashed curve corresponds to the Rainbow Ladder truncation scheme of equation (73), the solid curve to the improved kernel of equation (74), and the dotted curve is the asymptotic DA. This figure comes from Ref. [40].

3.2.1 Interpolating functions

In the case of the quark propagator, it has been chosen [40] to use a parameterisation involving complex conjugates poles:

$$S(k) = \sum_j^N \left[\frac{z_j}{i\gamma \cdot k + m_j} + \frac{z_j^*}{i\gamma \cdot k + m_j^*} \right], \quad (76)$$

where z_j and m_j are fitted on the grids of solutions. Fits are satisfactory for $N \geq 2$.

The functions associated with the Dirac structure of the pion Bethe-Salpeter amplitude (69) can be described using the so-called Nakanishi representation [145]:

$$\chi(k, P) = \mathcal{N} \int_{-1}^1 dz \int_0^\infty d\gamma \frac{\varphi_l^{[n]}(z, \gamma)}{(\gamma + \tilde{m}^2 - \frac{1}{4}m_H^2 - k^2 - P \cdot kz - i\epsilon)^{n+2}}, \quad (77)$$

with m_H being the mass of the considered hadron, \mathcal{N} a normalisation constant, \tilde{m} the mass of the constituents, and $\varphi_l^{[n]}(z, \gamma)$ is such that:

$$\lim_{\gamma \rightarrow \infty} \frac{\varphi_l^{[n]}(z, \gamma)}{\gamma^n} = 0. \quad (78)$$

The Nakanishi representation has been used in modern Dyson-Schwinger and Bethe-Salpeter studies of mesons, see *e.g.* Refs. [40, 146]. For instance, the authors of Ref. [40] split the functions E_π , F_π , and G_π into infrared and ultraviolet dominant contributions, and parameterise them using the Nakanishi representations. This method has allowed the computation of the pion DA, yielding a significantly wider distribution in terms of the momentum fraction than the asymptotic one, as shown on figure 7. Very recently, the same approach has been also followed to compute distribution amplitudes for bound-states involving strange and charm quarks [147, 148].

3.2.2 An algebraic model

The Nakanishi representation has been the starting point of an algebraic model suggested in Ref. [40], for both the quark propagator and the Bethe-Salpeter amplitude. Focusing on the

γ_5 term of the Bethe-Salpeter amplitude, the algebraic model yields:

$$S(p) = [-i\gamma \cdot p + M] \Delta_M(p^2), \quad (79)$$

$$\Delta_M(s) = \frac{1}{s + M^2}, \quad (80)$$

$$\Gamma_\pi(k, P) = i\gamma_5 \frac{M}{f_\pi} M^{2\nu} \int_{-1}^{+1} dz \rho_\nu(z) [\Delta_M(k_{+z}^2)]^\nu, \quad (81)$$

$$\rho_\nu(z) = \frac{1}{\sqrt{\pi}} \frac{\Gamma(\nu + 3/2)}{\Gamma(\nu + 1)} (1 - z^2)^\nu, \quad (82)$$

$$k_{+z} = k - \left(\frac{1-z}{2} - \eta \right) P. \quad (83)$$

Two parameters can be identified here⁴: ν which controls the shape of the pion Bethe-Salpeter amplitude and M which can be seen as an effective dressed quark mass. For $\nu = 1$, the analytic computation of the pion DA with this algebraic model is possible and leads to the asymptotic results [40]. Indeed, the pion DA defined in equation (19) can be seen as the projection of the Bethe-Salpeter wave function:

$$f_\pi \varphi_\pi(u) = \text{Tr} \left[Z_2 \int \frac{d^4 k}{(2\pi)^4} \delta(k_\eta \cdot n - uP \cdot n) \gamma \cdot n \gamma_5 \chi_\pi(k, P) \right], \quad (84)$$

k_η being defined in equation (68).

The results obtained for the pion DA are very encouraging, both numerically and analytically. Indeed, the algebraic parameterisation based on a simple Nakanishi representation (79)-(83) allows to compute analytically the asymptotic pion DA. Then fitting the parameters of equations (76) and (77) on the numerical solution of the DSEs provides a more realistic model for the pion DA, deforming the asymptotic one. A similar approach has been developed in Ref. [42] for GPDs. The idea is to use the algebraic parameterisation to highlight the main features of GPD modelling through the Nakanishi representation, paving the way for numerical computations based on equations (76) and (77).

4 Covariant computation of the pion GPD

4.1 Pion GPD Mellin moments

In this section, we review the modelling approach, within the previously described DSEs-BSE framework, used in Ref. [42] and references therein, based on a covariant computation of a non-perturbative matrix element which is generally performed through the so-called impulse approximation.

4.1.1 Local Impulse Approximation

Widely used to compute form factors, the impulse approximation corresponds in practice to model the considered matrix element using a triangle diagram as shown on figure 8 (e.g. see refs. [23, 24, 35–39]). However, this approximation cannot be applied directly to the GPD itself, due to the fact that, contrary to the form factor, the GPD is defined through a non-local matrix element. Consistently modelling this operator is not a trivial task, but the problem of non-locality can be circumvented. Indeed, as seen in equation (30), the Mellin moments of the pion GPD are directly proportional to a *local* matrix element in terms of the covariant local twist-two operators in equation (32). Yet, as emphasised in section 3, working in a DSEs-BSE framework means

⁴We remind the reader that the physics cannot depends on η because of translational invariance.

working in the Landau gauge, and thus one should take the covariant derivative instead of the partial one in equation (30). Expanding the covariant derivative leads to:

$$(\overleftrightarrow{D} \cdot n)^m = \frac{1}{2^m} \sum_{j=0}^m \binom{m}{j} (\overrightarrow{\partial} \cdot n - n \cdot \overleftarrow{\partial})^j (2ig n \cdot A)^{m-j}, \quad (85)$$

where the gluon contributions explicitly appears. However, the choice done here is to focus only on the term $j = m$, which corresponds to neglect the gauge link in the definition of the GPDs. The reader may find this a bold approximation, but it has been argued in Ref. [149] that the gauge link in twist-two operators along the lightcone brings only numerically negligible contributions.

The overall normalisation of the triangle diagram is controlled by the local twist-two operator. A normalisation condition of the Bethe-Salpeter amplitude based on charge conservation in the ladder approximation has been introduced by Mandelstam [150]. It relies on the computation of a pion form factor at vanishing momentum transfer within the impulse approximation. The value of the form factor is then fixed to 1. Consequently, as the form factor is the Mellin Moment of the GPD H for $m = 0$, it consists in fixing $\mathcal{M}_0(0, 0)$ to 1. Using the Ward-Takahashi identity (WTI):

$$i\Delta^\mu \Gamma_\mu(k + \frac{\Delta}{2}, k - \frac{\Delta}{2}) = S^{-1}(k + \frac{\Delta}{2}) - S^{-1}(k - \frac{\Delta}{2}), \quad (86)$$

Mandelstam's condition was shown [134, 151] to be equivalent to the canonical normalisation of the Bethe-Salpeter amplitude given in equation (70).

4.1.2 Computations of Mellin Moments

Following the Mandelstam approach which ensures charge conservation, the $m = 0$ local twist-two operator is assimilated to the vector current vertex Γ_μ . Higher- m operators are based on the first one, taking into account the action of the $(i\overleftrightarrow{D} \cdot n)^m$ on the incoming and outgoing quarks. In the algebraic model presented in Sec. 3.2.2, when applied to the quark fields, these operators yield: $(k \cdot n)^m$. Consequently, the computation of the Mellin moments $\mathcal{M}_m(\xi, t)$ of the pion quark GPD leads to:

$$\begin{aligned} 2(P \cdot n)^{m+1} \mathcal{M}_m(\xi, t) &= \text{Tr}_{\text{CFD}} \left[\int \frac{d^4 k}{(2\pi)^4} (k \cdot n)^m \tau_- i\bar{\Gamma}_\pi \left((1-\eta) \left(k + \frac{\Delta}{2} \right) + \eta(k-P), P + \frac{\Delta}{2} \right) \right. \\ &\quad S(k + \frac{\Delta}{2}) i n \cdot \Gamma(k + \frac{\Delta}{2}, k - \frac{\Delta}{2}) S(k - \frac{\Delta}{2}) \\ &\quad \left. \tau_+ i\Gamma_\pi \left(\eta(k-P) + (1-\eta) \left(k - \frac{\Delta}{2} \right), P - \frac{\Delta}{2} \right) S(k-P) \right], \end{aligned} \quad (87)$$

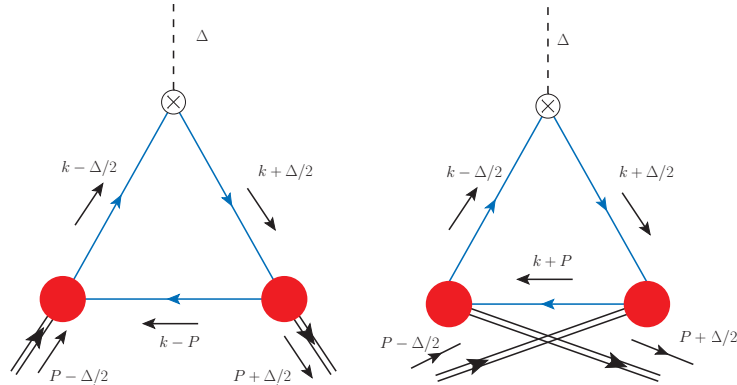


Figure 8: Triangle diagram approximation. Left-hand side: case of the quark GPD. Right-hand side: case of the anti-quark GPD.

for the leftmost diagram of figure 8 (a similar equation works for the rightmost one), where S and Γ_π have been defined in equations (79) and (81), respectively. $n \cdot \Gamma(k + \frac{\Delta}{2}, k - \frac{\Delta}{2})$ stands for the dressed quark photon vertex projected on the lightcone, and the τ^\pm are linear combinations of the Pauli matrices τ^i :

$$\tau^\pm = \tau^1 \pm i\tau^2. \quad (88)$$

To ensure the normalisation of the pion GPD computed in the impulse approximation, one need to use a vertex and a propagator consistent with the WTI (86). Relying on equation (79) for the quark propagator, the WTI yields:

$$S^{-1}(k + \frac{\Delta}{2}) - S^{-1}(k - \frac{\Delta}{2}) = i\Delta \cdot \gamma, \quad (89)$$

and thus, the minimal Ansatz required to fulfil the normalisation condition is $\Gamma^\mu = \gamma^\mu$. Then, the DSEs-BSE inspired algebraic parametrisation in equations (79-83) can be applied to (87) (details of the computation can be found in Ref. [42, 153]) and leads to:

$$\begin{aligned} \mathcal{M}_m(\xi, t) &= \frac{M^2}{2\pi^2 f_\pi^2} \int_0^1 dx dy du dv dw \int_{-1}^{+1} dz dz' \delta(x+y+u+v+w-1) x^{\nu-1} y^{\nu-1} \rho(z) \rho(z') \\ &\quad \frac{M^{4\nu}}{2} \left[\frac{\Gamma(2\nu+1)}{\Gamma(\nu)^2} \left((f\Delta \cdot n + gP \cdot n \left(\left(\frac{\Delta}{2} \right)^2 - P^2 \right) - 2P \cdot n \left(\frac{\Delta}{2} \right)^2 \right) \frac{1}{(M')^{2\nu+1}} \right. \\ &\quad + \frac{\Gamma(2\nu)}{\Gamma(\nu)^2} \frac{1}{2} \left(P \cdot n + \frac{\Delta}{2} \cdot n \right) \delta(v) \frac{1}{(M')^{2\nu}} + \frac{\Gamma(2\nu)}{\Gamma(\nu)^2} \frac{1}{2} \left(P \cdot n - \frac{\Delta}{2} \cdot n \right) \delta(w) \frac{1}{(M')^{2\nu}} \\ &\quad \left. + \frac{\Gamma(2\nu)}{\Gamma(\nu)^2} (f\Delta \cdot n + gP \cdot n) \delta(u) \frac{1}{(M')^{2\nu}} \right] \frac{(f\Delta \cdot n + gP \cdot n)^m}{2(P \cdot n)^{m+1}} \end{aligned} \quad (90)$$

where:

$$f = f(x, y, v, w, z, z') = \frac{1}{2} \left(-\frac{1+z'}{2} y + \frac{1+z}{2} x + v - w \right), \quad (91)$$

$$g = g(x, y, u, z, z') = \left(\frac{1-z'}{2} \right) y + x \frac{1-z}{2} + u, \quad (92)$$

$$\begin{aligned} M'^2(t, P^2, x, y, u, v, w, z, z') &= M^2 + \frac{t}{4} \left(-4f^2 + y \left(\frac{1+z'}{2} \right)^2 + x \left(\frac{1+z}{2} \right)^2 + v + w \right) \\ &\quad + P^2 \left(-g^2 + \left(\frac{1-z'}{2} \right)^2 y + \left(\frac{1-z}{2} \right)^2 x + u \right). \end{aligned} \quad (93)$$

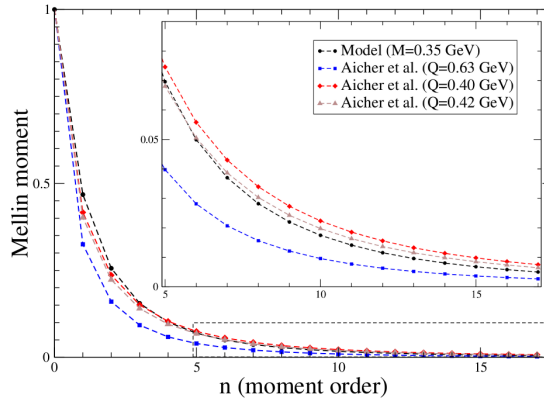


Figure 9: Mellin moments from equation (90) and obtained with the parameterisation of Ref. [152] run with DGLAP equation down to $Q = 0.40$ GeV and 0.42 GeV.

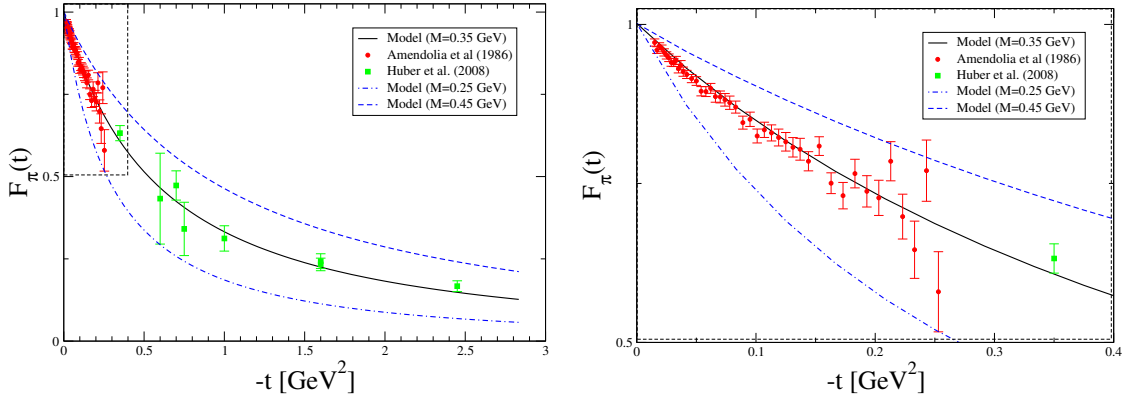


Figure 10: Left-hand side: the pion form factor F_π computed at $M = 0.35$ GeV (solid black line), 0.25 GeV (dot-dashed blue line) and 0.45 GeV (dashed blue line), with $\nu = 1$ for the three cases. Experimental data are taken from Ref. [154, 155]. Right-hand side: zoom of the dashed square in the leftmost plot allowing to emphasise the constraint provided by the large number of data points in the low-momentum region.

A similar expression can be derived for the rightmost diagram of figure 8 and both can be numerically evaluated to produce, for instance, the results plotted in figure 9.

4.1.3 Comparison to available data

Unfortunately, no experimental data are currently available for off-forward kinematics on a pion target, despite some studies on virtual targets [117]. Therefore, the present model can be compared only to PDF and form factors experimental data.

Owing to equation (29), the form factor can be computed by taking $m = 0$ in equation (90). In this approach, two parameters enter the game, as explained in section 3.2.2: ν is fixed to 1 and only M remains as a free parameter, which drives the t -behaviour of the model. This can be easily highlighted since after proper normalisation, equation (90) can be explicitly written in terms of $\theta = t/M^2$, instead of t and M . As argued in Ref. [42], the fit of the $m = 0$ moment to the available experimental data of Refs. [154, 155] allows for a precise determination of the parameter M , although the interest of such a fit is limited here, as our main purpose is to explore the possibilities offered by the DSE framework with regard to GPDs modelling. However, figure 10 shows that data are well described for $M \simeq 0.35$ GeV, which is a typical constituent quark mass. The sensitivity of the model with respect to M is highlighted by plotting two additional curves: one for $M = 0.25$ GeV and one for $M = 0.45$ GeV. The reader should note at this point that the form factor is providing a mass scale to the algebraic model, whereas when solving DSEs, the mass scale is intrinsic to the result.

The charge radius of the pion can also be determined here. The NA7 collaboration gives in Ref. [154] its experimental result:

$$\langle r_\pi^2 \rangle^{\text{exp}} = -6 \frac{dF_\pi}{dt} \Big|_{t=0} = 0.439 \pm 0.008 \text{ fm}^2. \quad (94)$$

The model would reach agreement with the NA7 Collaboration value for $M = 339 \pm 3$ MeV, which is close to the choice of $M = 350$ MeV.

Besides the pion form factor, the pion PDF has also been measured in the large- x region. Recent analyses taking into account gluon resummation [152] have provided the community with phenomenological parameterisations of the pion PDF. Consequently, it is possible to compute the Mellin moments of these phenomenological parameterisations, and to compare them with the ones computed in equation (90). However, the comparison can be done only at the same scale, and

the scale of the Mellin moments of equation (90) is *a priori* unknown. Moreover, as the PDF is taken at $\theta = 0$, the dependence in M , the only mass scale directly available, vanishes. The idea developed in Ref. [42] is thus to consider the scale μ_F as a free parameter. The Mellin moments of the phenomenological parameterisations of Ref. [152] have thus been evolved to lower scales. The relevant scale is then selected when the evolved phenomenological Mellin moments are in agreement with the ones computed through equation (90). As shown on figure 9 this corresponds to a low scale, close to the one chosen for M and thus highlighting the consistency of this approach.

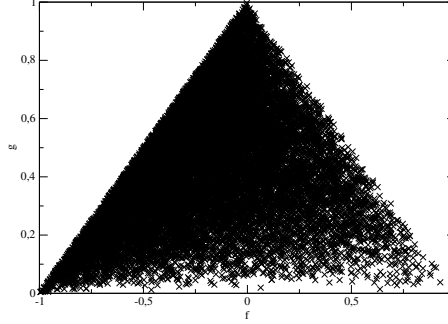


Figure 11: Right-hand side: Values of f and g when generating the Feynman parameters in a Monte-Carlo approach using 2.10^5 points. The shape of a half-rhombus clearly appears.

4.2 From Mellin moments to GPDs

Going from the Mellin moments to the pion GPD itself is *a priori* possible through the so-called Mellin-Barnes inverse transform [108]. However, this technique has been performed for models much simpler than the integrals in equations (90) only, and is hardly practicable here. Therefore, one should turn to other approaches.

4.2.1 Tensorial structure and Double Distributions

Instead, one can try to express the Mellin moments of equation (90) in the same way as in equation (47), in order to identify the DDs $F^q(\beta, \alpha, t)$ and $G^q(\beta, \alpha, t)$. This can actually be done, providing that one can identify the relevant variable β and α with the good support Ω , described in equation (45). From equation (90), the natural candidates are:

$$\begin{cases} \beta &= g \\ \alpha &= -f \end{cases}, \quad (95)$$

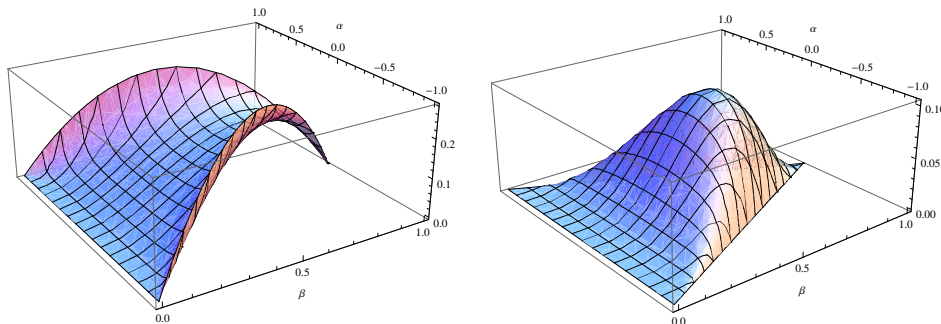


Figure 12: DDs F for $\nu = 1$ (left-hand side) and $\nu = 2$ (right-hand side).

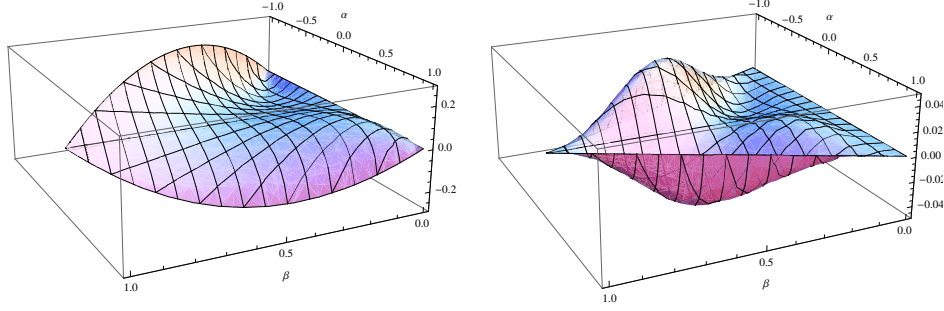


Figure 13: DDs G for $\nu = 1$ (left-hand side) and $\nu = 2$ (right-hand side).

where f and g have been defined in equations (91) and (92). The proof that f and g describe actually a half-rhombus can be found in [42]. But it is plain when looking at figure 11. Identifying the DDs $F^q(\beta, \alpha, t)$ and $G^q(\beta, \alpha, t)$ requires then a change of variables from the Feynman parameters to the DD variables β and α , *i.e.* following the pattern:

$$\int_0^1 dx dy du dv dw \int_{-1}^{+1} dz dz' \delta(x+y+u+v+w-1) \phi(x, y, u, v, w, z, z') = \int_{\Omega} d\beta d\alpha \Phi(\beta, \alpha). \quad (96)$$

Such a change of variable is non-trivial, but has been identified and performed in Ref. [42] leading to the DDs illustrated in figures 12 and 13 for $t = 0$.

4.2.2 GPDs reconstruction: successes and weaknesses

From the DDs, it is possible to compute the pion GPD through the relation (46). The results for $\nu = 1$, $\xi \geq 0$ and $t = 0$ yields in the DGLAP region:

$$\begin{aligned} H_{x \geq \xi}^u(x, \xi, 0) = & \frac{48}{5} \left\{ \frac{3(-2(x-1)^4(2x^2 - 5\xi^2 + 3) \log(1-x))}{20(\xi^2 - 1)^3} \right. \\ & + \frac{3 \left(+4\xi(15x^2(x+3) + (19x+29)\xi^4 + 5(x(x(x+11) + 21) + 3)\xi^2) \tanh^{-1} \left(\frac{(x-1)\xi}{x-\xi^2} \right) \right)}{20(\xi^2 - 1)^3} \\ & + \frac{3(x^3(x(2(x-4)x + 15) - 30) - 15(2x(x+5) + 5)\xi^4) \log(x^2 - \xi^2)}{20(\xi^2 - 1)^3} \\ & + \frac{3(-5x(x(x+2) + 36) + 18)\xi^2 - 15\xi^6) \log(x^2 - \xi^2)}{20(\xi^2 - 1)^3} \\ & + \frac{3(2(x-1)((23x+58)\xi^4 + (x(x(x+67) + 112) + 6)\xi^2 + x((5-2x)x + 15) + 3))}{20(\xi^2 - 1)^3} \\ & + \frac{3((15(2x(x+5) + 5)\xi^4 + 10x(3x(x+5) + 11)\xi^2) \log(1 - \xi^2))}{20(\xi^2 - 1)^3} \\ & \left. + \frac{3(2x(5x(x+2) - 6) + 15\xi^6 - 5\xi^2 + 3) \log(1 - \xi^2)}{20(\xi^2 - 1)^3} \right\}, \quad (97) \end{aligned}$$

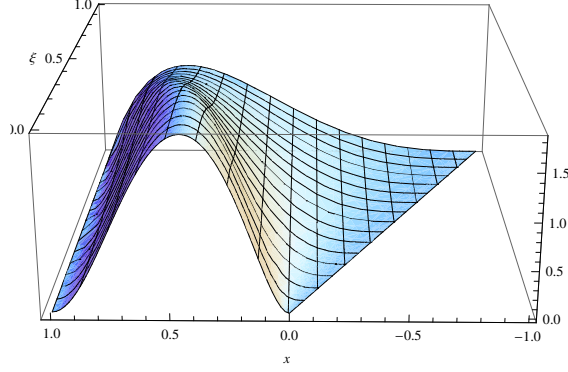


Figure 14: The pion GPD H^q computed for $\nu = 1$ at vanishing t .

and:

$$\begin{aligned}
H_{|x| \leq \xi}^u(x, \xi, 0) = & \frac{48}{5} \left\{ \frac{6\xi(x-1)^4 (-(2x^2 - 5\xi^2 + 3)) \log(1-x)}{40\xi(\xi^2 - 1)^3} \right. \\
& + \frac{6\xi(-4\xi(15x^2(x+3) + (19x+29)\xi^4 + 5(x(x(x+11)+21)+3)\xi^2) \log(2\xi))}{40\xi(\xi^2 - 1)^3} \\
& + \frac{6\xi(\xi+1)^3 ((38x+13)\xi^2 + 6x(5x+6)\xi + 2x(5x(x+2)-6) + 15\xi^3 - 9\xi + 3) \log(\xi+1)}{40\xi(\xi^2 - 1)^3} \\
& + \frac{6\xi(x-\xi)^3 ((7x-58)\xi^2 + 6(x-4)x\xi + x(2(x-4)x+15) + 15\xi^3 + 75\xi - 30) \log(\xi-x)}{40\xi(\xi^2 - 1)^3} \\
& + \frac{3(\xi-1)(x+\xi)(4x^4\xi - 2x^3\xi(\xi+7) + x^2(\xi((119-25\xi)\xi-5)+15))}{40\xi(\xi^2 - 1)^3} \\
& \left. + \frac{3(\xi-1)(x+\xi)(x\xi(\xi(71\xi+5)+219)+9) + 2\xi(\xi(2\xi(34\xi+5)+9)+3)}{40\xi(\xi^2 - 1)^3} \right\}, \quad (98)
\end{aligned}$$

in the ERBL one. These results are illustrated on figure 14. Equations (97) and (98) deserve several comments. First, several properties listed in section 2 are fulfilled as a direct consequence of the DD properties. It is the case of the support property, the parity in ξ , and the polynomiality property, despite the presence of logarithms in the contributions of the DGLAP and ERBL region to final results. The forward limit can be computed, leading to the following formula for the PDF computed in the triangle diagram approach:

$$q_{\pi}^{\text{Tr}}(x) = \frac{72}{25} \left((30-15x+8x^2-2x^3)x^3 \log x + (3+2x^2)(1-x)^4 \log(1-x) + (3+15x+5x^2-2x^3)x(1-x) \right). \quad (99)$$

The result on the pion PDF is analysed in section 6.

Still one property is not fulfilled here: the positivity. Indeed, as $q_{\pi}^{\text{Tr}}(x) \rightarrow 0$ when $x \rightarrow 0$, one should have:

$$|H(x, \xi, t)| \leq \sqrt{H\left(\frac{x-\xi}{1-\xi}, 0, 0\right) H\left(\frac{x+\xi}{1+\xi}, 0, 0\right)} \rightarrow 0 \text{ when } x \rightarrow \xi. \quad (100)$$

Thus, H^q should vanish on the line $x = \xi$. From figure 14, this is obviously not the case. The reason why the positivity property is violated in this approach remains unknown, but one cannot exclude that it might be a facet of the algebraic model used for the computations and that, when using the full solution of the DSEs, the problem might not exist any more.

5 Chiral properties and soft pion theorem

As stated above, the pion GPD model building cannot be constrained by experimental results for an off-forward kinematics. However, the verification of the soft pion theorem is a challenging test that a proper model must pass beyond the forward kinematics, at $\xi = 1$ and $t = 0$. We stress now the minimal requirements needed for a DSE-BSE inspired model to succeed in fulfilling the theorem.

5.1 Consequences of the Axial-Vector Ward Takahashi Identity

Both $\Gamma_\mu^5(k, P)$ and $\Gamma_5(k, P)$ can be written in terms of the pion Bethe-Salpeter amplitude $\Gamma_\pi^j(k, P)$ [136]:

$$\begin{aligned}\Gamma_\mu^{5j}(k, P) &= \frac{\tau^j}{2} \gamma_5 [\gamma_\mu F_{AV}(k, P) + \gamma \cdot k k_\mu G_{AV}(k, P) - \sigma_{\mu\nu} k^\nu H_{AV}(k, P)] \\ &\quad + \tilde{\Gamma}_\mu^{5j}(k, P) + \frac{f_\pi P_\mu}{P^2 + m_\pi^2} \Gamma_\pi^j(k, P),\end{aligned}\tag{101}$$

and

$$\begin{aligned}i\Gamma^{5j}(k, P) &= \frac{\tau^j}{2} \gamma_5 [iE_A(k, P) + \gamma \cdot P F_A(k, P) + \gamma \cdot k k \cdot P G_A(k, P) \\ &\quad + \sigma_{\mu\nu} k^\nu P^\mu H_A(k, P)] + \frac{\rho_\pi}{P^2 + m_\pi^2} \Gamma_\pi^j(k, P),\end{aligned}\tag{102}$$

with ρ_π being a constant and j the isospin index. E, F, G and H are scalar functions with no singularities at $P^2 = -m_\pi^2$. $\tilde{\Gamma}_\mu^{5j}$ is also a non-singular contribution to the axial-vector vertex at the pion mass. Therefore, working in the chiral limit, one can relate the axial-vector and axial vertices to the Bethe-Salpeter amplitude through:

$$\lim_{P \rightarrow 0} P^\mu \Gamma_\mu^{5j}(k, P) = f_\pi \Gamma_\pi^j(k, 0),\tag{103}$$

$$\lim_{P^2 \rightarrow 0} iP^2 \Gamma_5^j(k, P) = \rho_\pi \Gamma_\pi^j(k, P)|_{P^2=0}.\tag{104}$$

Injecting equation (103) within the AVWTI defined in equation (71) one gets:

$$f_\pi \Gamma_\pi^j(k, 0) = i\gamma_5 \frac{\tau^j}{2} S^{-1}(k) + iS^{-1}(k) \gamma_5 \frac{\tau^j}{2},\tag{105}$$

in the chiral limit. Using the expansion of $\Gamma_\pi^j(k, 0)$ in equation (69) and of $S^{-1}(k)$ in equation (60), it is possible to simplify equation (105) in a Goldberger-Treimann-like relation [136, 156]:

$$f_\pi E_\pi(k, 0) = B_q(k^2) = M_q(k^2) A_q(k^2).\tag{106}$$

Consequently, the internal structure of the pion is directly related to the running dressed quark mass M_q .

5.2 Soft Pion Theorem

In the chiral limit, the AVWTI plays a key role in recovering the so-called soft pion theorem described in section 2. As it has been highlighted in Ref. [43], when properly taken into account, the AVWTI allows the computation of the pion GPDs to fulfil the soft pion theorem within the impulse approximation. To show this, one first has to look at the kinematics in which the soft pion theorem applies:

$$\begin{aligned}\xi = 1 &\Rightarrow \Delta^+ = -2P^+, \\ m_\pi^2 = 0 &\Rightarrow (P + \frac{\Delta}{2})^2 = 0 \Rightarrow \Delta_\perp = 0 \Rightarrow P^- = 0, \\ t = 0 &\Rightarrow \Delta^- = 0.\end{aligned}\tag{107}$$

Therefore, on figure 8, the momentum of the outgoing pion $p_2 = P + \frac{\Delta}{2}$ vanishes, whereas the incoming pion is a lightlike particle as $p_1 = 2P^+$. At vanishing momentum, one can consider the Bethe-Salpeter amplitude of the outgoing pion as the limit of the axial-vector vertex as shown in equation (103). On the other hand, the momentum of the incoming pion being such that $p_1^2 = (2P)^2 = \Delta^2$ allows one to use equation (104) to express the Bethe-Salpeter amplitude in terms of the axial vertex. More formally, one can write:

$$\mathcal{M}_m(\xi = 1, t = 0) = \lim_{t \rightarrow 0} \lim_{\xi \rightarrow 1} \lim_{m_\pi^2 \rightarrow 0} \text{Tr}_{\text{CFD}} \left[\int \frac{d^4 k}{(2\pi)^4} \frac{(k \cdot n)^m \tau_-}{2(P \cdot n)^{m+1}} i \frac{(P + \frac{\Delta}{2})^\mu}{f_\pi} \bar{\Gamma}_\mu^5 \left((k - P), P + \frac{\Delta}{2} \right) \right. \\ \left. \times S(k - P) i n \cdot \Gamma(k - P, k + P) S(k + P) \tau_+ i \frac{i(P^2 + (\frac{\Delta}{2})^2)}{\rho_\pi} \Gamma_5 \left((k + P), P - \frac{\Delta}{2} \right) S(k - P) \right]. \quad (108)$$

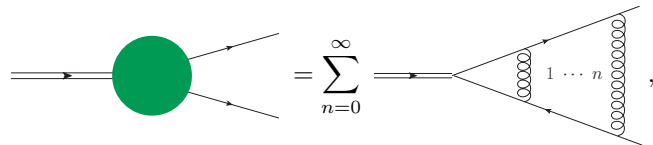
Injecting the AVWTI (71) in equation (108) and taking the chiral limit leads to:

$$(P + \frac{\Delta}{2})^\mu \bar{\Gamma}_\mu^5 \left((k - P), P + \frac{\Delta}{2} \right) = i \gamma_5 S^{-1}(k - P) + S^{-1}(k - P) i \gamma_5, \quad (109)$$

for $P + \frac{\Delta}{2} \rightarrow 0$. Then injecting equation (109) into equation (108), one gets:

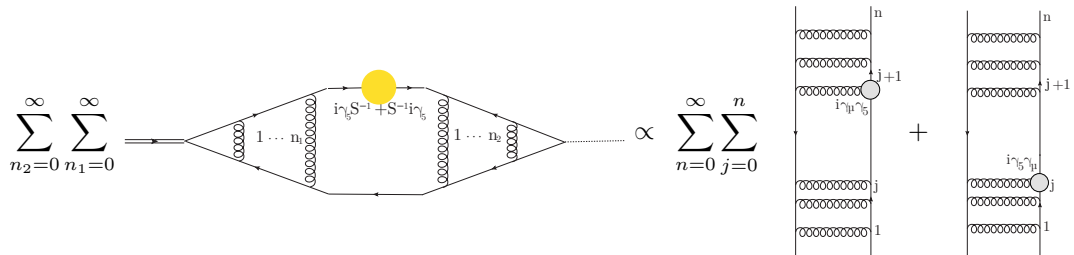
$$\mathcal{M}_m(\xi = 1, t = 0) = \lim_{t \rightarrow 0} \lim_{\xi \rightarrow 1} \text{Tr}_{\text{CFD}} \left[\int \frac{d^4 k}{(2\pi)^4} \frac{(k \cdot n)^m \tau_-}{2(P \cdot n)^{m+1}} \frac{i}{f_\pi} \right. \\ \times \left(i \gamma_5 i n \cdot \Gamma(k - P, k + P) S(k + P) \tau_+ i \frac{i(P^2 + (\frac{\Delta}{2})^2)}{\rho_\pi} \Gamma_5 \left((k + P), P - \frac{\Delta}{2} \right) S(k - P) \right. \\ \left. \left. + i \gamma_5 S(k - P) i n \cdot \Gamma(k - P, k + P) S(k + P) \tau_+ i \frac{i(P^2 + (\frac{\Delta}{2})^2)}{\rho_\pi} \Gamma_5 \left((k + P), P - \frac{\Delta}{2} \right) \right) \right]. \quad (110)$$

Consequently, one has to compute two contributions containing only two dressed vertices instead of three. To do so, it is necessary to “unfold” these vertices. Both of them fulfil an inhomogeneous Bethe-Salpeter equation, and therefore in the RL approximation of equation (73), they can be seen as an infinite sum of gluons ladder:



$$= \sum_{n=0}^{\infty} \text{diagram with } n \text{ gluon ladders}, \quad (111)$$

where n stands for the number of considered gluon ladders, and $n = 0$ correspond to the “undressed” case, *i.e.* when no gluon is exchanged between the two quarks. The Dirac matrices γ_5 in equation (110) are thus trapped between two sets of gluon ladders. Nevertheless, relabelling the series leads to the following contributions:



$$\sum_{n_2=0}^{\infty} \sum_{n_1=0}^{\infty} \text{diagram} \propto \sum_{n=0}^{\infty} \sum_{j=0}^n \text{diagram 1} + \sum_{n=0}^{\infty} \sum_{j=0}^n \text{diagram 2}, \quad (112)$$

where n stands now for the total number of gluon ladder in the diagram, and the j index is such that the AVWTI is inserted between the j^{th} and the $(j+1)^{th}$ gluon ladder. As γ_5 and γ^μ anticommute, for a given n , only two contributions on the right-hand side of equation (112) do not cancel completely each other. In the case of the first ladder in equation (112) it is the contribution for $j = n$, whereas in the case of the second ladder, it is the one for $j = 0$. These two contributions have a very specific meaning. Indeed, in both case, one of the vertices is considered as “undressed”, as there is no gluon ladder between the insertion and the vertex itself. On the other hand, this analysis being valid for any n , one can resum the contributions for n from 0 to infinity. This is exactly what is done in equation (111), allowing one to get back the dressed vertex in the RL approximation. As a result, equation (110) yields:

$$\begin{aligned} \mathcal{M}_m(\xi = 1, t = 0) &= \lim_{t \rightarrow 0} \lim_{\xi \rightarrow 1} \text{Tr}_{\text{CFD}} \left[\int \frac{d^4 k}{(2\pi)^4} \frac{(k \cdot n)^m \tau_-}{2(P \cdot n)^{m+1}} \frac{i}{f_\pi} \right. \\ &\quad \times \left(i\gamma_5 i n \cdot \gamma S(k+P) \tau_+ i \frac{i(P^2 + (\frac{\Delta}{2})^2)}{\rho_\pi} \Gamma_5 \left((k+P), P - \frac{\Delta}{2} \right) S(k-P) \right. \\ &\quad \left. \left. + S(k-P) i n \cdot \Gamma(k-P, k+P) S(k+P) \tau_+ i \frac{i(P^2 + (\frac{\Delta}{2})^2)}{\rho_\pi} i(\gamma_5)^2 \right) \right]. \end{aligned} \quad (113)$$

Taking the limit $\xi \rightarrow 1$ and $t \rightarrow 0$ leads to $(P^2 + (\frac{\Delta}{2})^2) \rightarrow 0$. Thus in equation (113), the first contribution, depending on $\Gamma_5(k+P, P - \frac{\Delta}{2})$ can be written in terms of the pion Bethe-Salpeter amplitude through equation (104). The second one actually vanishes, due to the lack of poles in $\Gamma(k-P, k+P)$ when $(P^2 + (\frac{\Delta}{2})^2) \rightarrow 0$, *i.e.* there is no massless vector meson. One is therefore left with:

$$\mathcal{M}_m(1, 0) = \text{Tr}_{\text{CFD}} \left[\frac{1}{f_\pi} \int \frac{d^4 k}{(2\pi)^4} \frac{(k \cdot n)^m \tau_-}{2(P \cdot n)^{m+1}} \gamma_5 n \cdot \gamma S(k+P) \tau_+ \Gamma_\pi \left((k+P), P - \frac{\Delta}{2} \right) S(k-P) \right]. \quad (114)$$

Then, the following change of variables:

$$\begin{cases} p_1 &= 2P \\ k' &= k+P \end{cases}, \quad (115)$$

leads to:

$$\begin{aligned} \mathcal{M}_m(1, 0) &= \text{Tr}_{\text{CFD}} \left[\frac{1}{f_\pi} \int \frac{d^4 k'}{(2\pi)^4} \frac{(k' \cdot n - P \cdot n)^m \tau_-}{2(P \cdot n)^{m+1}} \gamma_5 n \cdot \gamma \tau_+ \chi_\pi(k', p_1) \right] \\ &= \text{Tr}_{\text{CFD}} \left[\frac{1}{f_\pi p_1 \cdot n} \int \frac{d^4 k'}{(2\pi)^4} \left(2 \frac{k' \cdot n}{p_1 \cdot n} - 1 \right)^m \gamma_5 n \cdot \gamma \tau_+ \chi_\pi(k', p_1) \right] \\ &= \text{Tr}_{\text{CFD}} \left[\int du (2u-1)^m \frac{1}{f_\pi} \int \frac{d^4 k'}{(2\pi)^4} \delta(u p_1 \cdot n - k \cdot n) \gamma_5 n \cdot \gamma \tau_+ \chi_\pi(k', p_1) \right] \\ &= \int du (2u-1)^m \varphi_\pi(u), \end{aligned} \quad (116)$$

where φ_π is the pion DA defined, as defined in equation (84) in terms of the Bethe-Salpeter wave function. As a continuous compactly supported function is uniquely defined by its Mellin moments, one can conclude that:

$$H_\pi^q(x, 1, 0) = \frac{1}{2} \varphi_\pi \left(\frac{1+x}{2} \right), \quad (117)$$

in agreement⁵ with the literature [7]. In terms of isovector and isoscalar GPDs, one gets back equation (20).

⁵Depending on the conventions used, an additional factor 1/2 may appear in the literature, like for instance in Ref. [48].

Summarising the proof above, one can say that the impulse approximation is compatible with the soft pion theorem in the *chiral limit*, under two main conditions. First, one has to work within a truncation scheme which fulfils the so-called AVWTI. Then, one can prove that the soft pion theorem is fulfilled when using the RL truncation scheme. One can expect that to go beyond the chiral limit, a more refined truncation scheme is needed, providing a way to better describe the Dynamical Chiral Symmetry Breaking than the RL approximation of equation (73). Indeed, from the proof presented above, we expect the fulfilment of the soft pion theorem by a DSE-BSE based GPD model, to be deeply related to the way the truncation scheme dynamically breaks chiral symmetry.

6 Beyond the impulse approximation

As seen in the previous sections, the impulse approximation allows the building of simple models of GPDs, which fulfil most of the theoretical constraints discussed in section 2. It is also consistent, in the relevant off-forward kinematic limit, with the soft pion theorem, within the RL truncation scheme and provided that the AVWTI is also verified. It remains nevertheless an approximation whose limitations can already be seen in the forward limit.

6.1 Forward kinematics implications

In the following, we will show how, according to Ref. [41], the valence-quark PDF appears distorted by the impulse approximation. Introducing the appropriate amendments, it is possible to go beyond this approximation highlight the basic features of the PDF.

6.1.1 Asymmetry of the PDF

Indeed, in the approach exposed in the previous section, one considers that the pion is composed of two effective dressed quarks. From discrete and isospin symmetries detailed in equations (12)-(18), it is possible to conclude that the two quark pion GPDs are such that:

$$H_{\pi^+}^u(x, \xi, t) = H_{\pi^+}^{\bar{d}}(x, \xi, t). \quad (118)$$

In the forward case, for the valence-quark PDF where neither sea-quark nor gluon contributions do not play any role, momentum conservation adds a strong constraint. Valence distributions are normalised to 1 and number densities become probability densities. Therefore, if one has a probability density to find a u quark carrying a momentum fraction x , then, a \bar{d} can be found with the same probability density but carrying a $1 - x$ momentum fraction. Together with equation (118), momentum conservation imposes the pion two-body PDF to be symmetric under the transformation $x \leftrightarrow (1 - x)$. On top of this, it has been also proved that, in a two-body framework, the forward limit for the GPD in the so-called overlap representation results in a symmetric PDF [43]. However, the results obtained in equation (99) slightly violate the $x \leftrightarrow (1 - x)$ symmetry, as it will also be shown on figure 16. Then, when computing the pion GPD within the covariant approach and impulse approximation, one necessarily misses an important piece of information.

6.1.2 Additional symmetrising Contributions

According to Ref. [41], the flaw in the valence-quark PDF comes from contributions related to gluons binding the quarks into the pion that, within the impulse approximation, are explicitly omitted. Therein, the drawback is discussed and the appropriate correction to the usual PDF definition within the impulse approximation is described. The discussion is made there in terms of the virtual Compton scattering amplitude in the RL truncation scheme. Ref. [41] presents a diagram analysis, which shows how the textbook *handbag* contribution can be approximated to the triangle diagram, typically the only retained. But it also shows how additional terms emerge and the role played by the latter in order to recover the basic features for the PDF.

Here, we will follow the alternative approach shown in Ref. [153] to both exhibit the failure of the impulse approximation and pinpoint the correct amendment in the forward limit, relying on the proper definition of the twist-two local operators. In the impulse approximation, the insertion of the twist-two local operators is solely done “*between*” two Bethe-Salpeter amplitudes, leading to the triangle diagram. Nonetheless, as suggested on figure 15, one can also imagine that the operators can be directly inserted “*inside*” the Bethe-Salpeter vertices, for either the incoming or outgoing hadrons. Precisely, such a direct insertion is needed to reproduce the omitted diagrams in the usual PDF computations within the impulse approximation [43, 153].

In order to figure out how these new contributions are related to the Bethe-Salpeter amplitude, one has to “unfold” the latter. Indeed, the RL kernel in equation (73) suggests that the Bethe-Salpeter amplitude is composed of a infinite number of gluon exchanges between the two quarks. In this view, it is then possible to insert the twist-two operator between any of these gluon exchanges. Therefore, the “squared” vertex can be considered as a sum over all the possible ways to include the local twist-two operators between two gluon ladders, *i.e.* :

The diagram shows a red square vertex on the left, representing a squared vertex. It is equated to a sum over $j=0$ to ∞ of a red circle vertex. The red circle vertex is connected to two gluon ladders. The first gluon ladder has a quark line with momentum k_j and a gluon line with momentum q_j . A cross symbol \otimes is placed on the quark line, indicating the insertion of a twist-two operator. The second gluon ladder has a quark line with momentum q_{j+1} and a gluon line with momentum q_{j+1} . The diagram is labeled (119).

where as in figure 8, the cross indicate the insertion of the twist two operators between the j^{th} and the $(j+1)^{th}$ gluons. In momentum space, this contribution can be written as:

$$n_\mu n_{\mu_1} \dots n_{\mu_m} O^{\{\mu, \mu_1 \dots \mu_m\}} \rightarrow (k \cdot n)^m i \Gamma(k - \frac{\Delta}{2}, k + \frac{\Delta}{2}) \cdot n, \quad (120)$$

for non-vanishing values of Δ . As before, $\Gamma(k - \frac{\Delta}{2}, k + \frac{\Delta}{2}) \cdot n$ denotes the projection of the vector current on the lightcone. As previously, this vertex has to fulfil the WTI (86). In the forward case, this leads to:

$$i\Gamma^\mu(k_j, k_j) = \frac{\partial S^{-1}}{\partial k_j^\mu}(k_j), \quad (121)$$

k_j being the quark momentum as defined in equation (119). Denoting q_j the momentum of the j^{th} gluon exchanged, momentum conservation imposes $k_{j+1} = k_j + q_{j+1}$. Therefore, being given that P , the pion total momentum and k , the relative momentum between the quarks are given, the relevant “internal variables” of the Bethe-Salpeter amplitude are the $\{q_j\}$ s. Therefore, one can formally rewrite the momenta k_j as:

$$k_j = k - \sum_{\ell=j+1}^{\infty} q_\ell. \quad (122)$$

The derivative of the inverse propagator can be now related to the propagator itself through:

$$\frac{\partial S}{\partial k_j^\mu}(k_j) = -S(k_j) \frac{\partial S^{-1}}{\partial k_j^\mu}(k_j) S(k_j), \quad (123)$$

we can next take advantage of the change of variable in equation (122) to, as follows,

$$\frac{\partial S}{\partial k_j^\mu}(k_j) = \frac{\partial S}{\partial k^\mu}(k_j), \quad (124)$$

let the derivative act on the outgoing momentum k instead of k_j . Then, as the derivative in equation (124) does not depend on j anymore, the infinite sum over all the possible insertions can

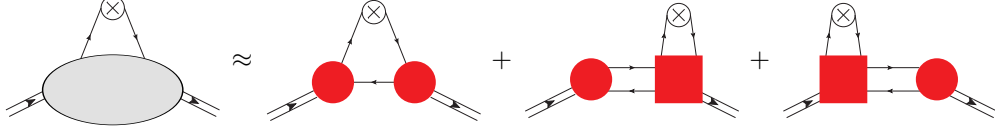
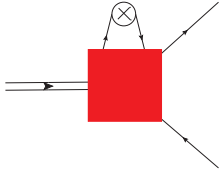


Figure 15: Additional contributions to the triangle diagrams. The circle vertices correspond to the Bethe-Salpeter amplitudes, whereas the squared vertices denote a new non-perturbative object related to the Bethe-Salpeter amplitude but on which the twist-two operators also act.

be reduced to the derivative of the Bethe-Salpeter amplitude itself:



$$= -\frac{1}{2}(k \cdot n)^m n^\mu \frac{\partial \Gamma_\pi^q}{\partial k^\mu}(k, P). \quad (125)$$

The factor $1/2$ stands here to avoid double counting: isospin and crossing symmetries authorize the definition of the GPD by an insertion only sticking either on the quark (as here) or on the anti-quark line; however, the derivative of the Bethe-Salpeter amplitude in (125) acts on all the propagators of both the quark and the antiquark lines in (119), both yielding the same result; then, one needs to correct for an spurious factor 2 in order to defining the additional proper contribution to the pion GPD.

6.1.3 Computations and results

We can now plug equation (125) for the *new* vertices in the additional contributions for pion PDF displayed in figure 15 and apply next the computation techniques developed in section 4. Owing to equation (81), the derivative of the Bethe-Salpeter amplitude yields:

$$\frac{\partial \Gamma_\pi^q}{\partial k^\mu}(k, P) = -2\nu \int dz \frac{M^{2\nu} \rho(z) (k^\mu - (\frac{1-z}{2} - \eta)P^\mu)}{\left[(k - (\frac{1-z}{2} - \eta)P)^2 + M^2 \right]^{\nu+1}}. \quad (126)$$

In the forward limit, both the two additional diagrams shown on figure 15 give the same results and one can thus define the additional contribution to the PDF Mellin moments as:

$$\mathcal{M}_m^{\text{ad}}(0, 0) = \text{Tr}_{\text{CFD}} \left[- \int \frac{d^4 k}{(2\pi)^4} \frac{(k \cdot n)^m}{2(P \cdot n)^{m+1}} \tau_- i \bar{\Gamma}_\pi(k, P) S(k) \tau_+ i n^\mu \frac{\partial \Gamma_\pi}{\partial k^\mu}(k, P) S(k - P) \right]. \quad (127)$$

Then, following the procedure described in section 4, one can obtain from this additional contribution a supplement to the DDs that had been previously computed from (90), denoted now $F^{\text{ad}}(\beta, \alpha, 0)$ and $G^{\text{ad}}(\beta, \alpha, 0)$. Using equations (46) and (21), these new terms result in the additional contribution to the pion PDF:

$$q_\pi^{\text{ad}}(x) = \int_{-1+x}^{1-x} d\alpha F^{\text{ad}}(x, \alpha, 0) = \frac{72}{25} \left(- (2x^3 + 4x + 9) (x-1)^3 \log(1-x) + x^3 (2x((x-3)x+5) - 15) \log(x) - x(x-1)(2x-1)((x-1)x-9) \right). \quad (128)$$

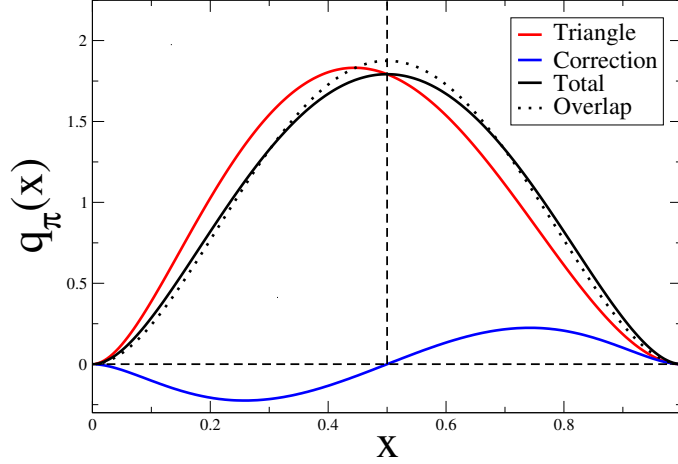


Figure 16: PDF contributions. In red the $q_\pi^{\text{Tr}}(x)$ coming from the triangle diagram, in blue the additional contribution taking into account the derivative of the Bethe-Salpeter amplitude $q_\pi^{\text{ad}}(x)$, and in black solid line the total PDF $q_\pi^{\text{tot}}(x)$. The black dotted line corresponds to PDF obtained by applying the overlap representation that will be discussed in the next section.

Adding this component to the one coming from the impulse approximation (99), one gets the total PDF:

$$q_\pi^{\text{tot}}(x) = q_\pi^{\text{Tr}}(x) + q_\pi^{\text{ad}}(x) = \frac{72}{25} \left((-2x(1-x) - 3x + 15)x^3 \log(x) - (-2x(1-x) - 3(1-x) + 15)(x-1)^3 \log(1-x) - 2x(x-1)((x-1)x + 6) \right), \quad (129)$$

which, as a remarkable feature, is symmetric under the $x \leftrightarrow 1-x$ exchange. Then, the contribution from the two additional diagrams, including the “squared vertex” defined by (125), on figure 15, exactly cancels the asymmetry noticed before. This is illustrated by the black solid curve displayed in figure 16.

A few further remarks are appropriate here. The contribution resulting from the derivative of the Bethe-Salpeter amplitude does leave the pion form factor unaltered. This is plain on figure 16, as it is antisymmetric within the $x \leftrightarrow 1-x$ exchange. Therefore, the normalisation of the PDF can be determined only through the triangle diagram contribution, which is fully consistent with Mandelstam normalisation procedure, as explained in section 3. One can also check the momentum sum rule which here yields:

$$\int_0^1 dx [q_\pi^{\text{Tr}}(x) + q_\pi^{\text{ad}}(x)] = \frac{117}{250} + \frac{8}{250} = \frac{1}{2}, \quad (130)$$

fully in agreement with a valence-quark two-body picture, as both quark and antiquark carry on average 1/2 of the total momentum. It is worthwhile to emphasise that the triangle diagram, by its own, is not able to fulfil this sum rule. Furthermore, in ref. [157], some corrections to the RL truncation originally used to define the PDF are included to make possible for some momentum its shifting from dressed quarks to sea-quarks and gluons and, thus, obtain a realistic PDF beyond the two-body picture which compares well with available experiment. A last comment on the large- x behaviour for the present PDF model is also in order. Indeed, one is left with:

$$q_\pi^{\text{tot}}(x) = \frac{216}{5}(1-x)^2 + O((1-x)^3), \quad (131)$$

when $x \rightarrow 1$. This is in agreement with the power law derived through the parton model [158, 159].

Either in perturbative QCD [160, 161], or in Dyson-Schwinger equations computations [44, 162, 163], a large- x behaviour such that $q_\pi(x) \sim (1-x)^{2+\gamma}$ is predicted, with $\gamma > 0$.

6.2 Three-dimensional sketch of the pion

The additional diagrams including the vertex in equation (125) yield a new contribution to the pion GPD in the forward case which allows for the restoration of the $x \leftrightarrow 1-x$ symmetry. Its generalisation to the off-forward kinematics regime is a hard task and remains an open question. The relation of these additional terms with the positivity property, violated in our computations done within the impulse approximation, is also unclear. However, at vanishing ξ , as described in Ref. [43], one can obtain an approximated result for the GPD and its associated impact-parameter dependent distribution, see equation (43), which provides a qualitatively sound picture of the pion's dressed-quark structure at a hadronic scale. Indeed, one can write the non-skewed pion GPD as:

$$H_\pi^q(x, 0, t) = H_\pi^q(x, 0, 0) \mathcal{N}(t) C_\pi^q(x, t) F_\pi^q(t), \quad (132)$$

where $F_\pi^q(t)$ is the quark contribution to the pion form factor, $C_\pi^q(x, t)$ encodes the correlations between x and t , and $\mathcal{N}^q(t)$ is a normalisation factor such that:

$$1 = \mathcal{N}^q(t) \int dx H_\pi^q(x, 0, 0) C_\pi^q(x, t). \quad (133)$$

It is then possible to build an insightful pion GPD Ansatz based on the previous calculations. As already shown on figure 10, the impulse approximation provides a form factor in good agreement with experimental data. Yet, the vector current vertex can be appropriately dressed to account for its extended nature [34]. The latter is proved not to generate new (x, t) correlations and only affect slightly the t -behaviour of the form factor, such that the mass-scale M for the algebraic model, see equations (79-83), appears just shifted from 0.35 to 0.40 GeV in order to reproduce experimental data [43]. The PDF $q_\pi^{\text{tot}}(x) = H_\pi^q(x, 0, 0)$ has been also computed in the previous section and the result is given in equation (129). Within this framework, the only missing piece is $C_\pi^q(x, t)$, which should not be identically one in realistic approaches [164].

In order to get sensible insights of the (x, t) correlations, computations of an additional F -type DD have been performed using the following approximation for the Mellin moments [43], which is a generalisation of equation (127):

$$\begin{aligned} \mathcal{M}_m^{\text{ad}}(\xi, t) &= \frac{1}{2} \int \frac{d^4 k}{(2\pi)^4} \text{Tr}_{\text{CDF}} \left[n \cdot \frac{\partial \bar{\Gamma}_\pi}{\partial k} \left(k + \frac{\Delta}{2}, P + \frac{\Delta}{2} \right) S(k - P) \Gamma_\pi \left(k - \frac{\Delta}{2}, P - \frac{\Delta}{2} \right) S \left(k - \frac{\Delta}{2} \right) \right. \\ &\quad \left. + \bar{\Gamma}_\pi \left(k + \frac{\Delta}{2}, P + \frac{\Delta}{2} \right) S(k - P) n \cdot \frac{\partial \Gamma_\pi}{\partial k} \left(k - \frac{\Delta}{2}, P - \frac{\Delta}{2} \right) S \left(k + \frac{\Delta}{2} \right) \right] \frac{(k \cdot n)^m}{(P \cdot n)^{m+1}}. \end{aligned} \quad (134)$$

This expression provides the proper forward limit, incorporating the contributions from the additional diagrams in figure 15, as can be easily seen by an explicit evaluation at $\Delta \rightarrow 0$ and comparison with equation (127). Nevertheless, the resulting non-forward GPD is also flawed by the approximated extension to the off-forward kinematics defined by (134). In particular, in the limit given by $\xi = 1$ and $t = 0$, equation (134) gives a non-vanishing contribution, whereas from the previous section, we expect this term to vanish. Indeed, the impulse approximation already provides the soft pion theorem in the RL truncation scheme, as soon as the AVWTI is well implemented. However, The results from (134) make possible a thoughtful study of the structure for the (x, t) correlations and, finally, lead to an additional component for the F -type DD such that the total $F^{\text{tot}}(\beta, \alpha, t)$ can be seen as:

$$\begin{aligned} F^{\text{tot}}(\beta, \alpha, t) &= F^{\text{Tr}}(\beta, \alpha, t) + F^{\text{ad}}(\beta, \alpha, t) \\ &= \phi^2(\beta, \alpha, t) \left[F^{\text{sym}}(\beta, \alpha) + \frac{t}{4M^2} V(\beta, \alpha) \phi(\beta, \alpha, t) \right], \end{aligned} \quad (135)$$

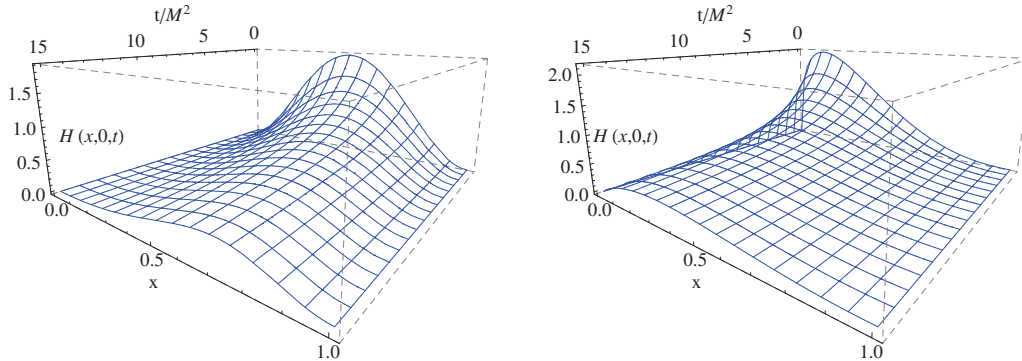


Figure 17: $H(x, 0, t)$ using the correlation model of equation (137). Left-hand side: Original scale $\mu_F = 0.51$ GeV. Right-hand side: Evolved GPD at scale $\mu_F = 2$ GeV. Plots are from Ref. [43].

where F^{sym} is the contribution leading to the symmetric PDF $q_\pi^{\text{tot}}(x)$, and ϕ is given by:

$$\phi(\beta, \alpha, t) = \frac{1}{1 + \frac{t}{4M^2}(1 + \alpha - \beta)(1 - \alpha - \beta)}. \quad (136)$$

Lightcone considerations (see Ref. [43]), suggest that $V(\beta, \alpha)$ shows a pathological behaviour, presumably due to the simple modelling done in equation (134).

These considerations allow an Ansatz for $C_\pi^q(x, t)$ based for simplicity on $\phi(\beta, \alpha = 0, t)$:

$$C_\pi^q(x, t) = \phi(x, 0, t)^2 = \frac{1}{\left(1 + \frac{t}{4M^2}(1 - x)^2\right)^2}, \quad (137)$$

which is shown [43] not to differ very much from the same obtained with a heuristic model for light-cone wave function applied to obtain the GPD in the overlap representation [164]. One should note that at large- x , $C_\pi^q(x, t) \rightarrow 1$, and thus, the perturbative behaviour previously highlighted remains. Using equation (132) it is then possible to compute the GPD itself. The result is shown on the left-hand side of figure 17. Starting from a symmetric distribution, as t grows, the GPD becomes more and more asymmetric, the maximum being shifted toward the large- x region. In addition, the distribution is also flattened as t grows. Evolution does not change this latter point significantly, but it shifts the entire distribution to the small- x region, as shown on the right-hand side of figure 17. The PDF is therefore no more symmetric. This can be easily understood, as evolution unravels the substructure of dressed quarks in terms of sea-quarks and gluons, which carry a smaller amount of the total pion momentum.

Equation (43) allows to compute the 3D dressed quark density in the transverse plane. As shown on figure 18, when x goes to 1, the distribution becomes narrower. Indeed, in this case, the considered parton carries most of the available momentum. Therefore, it defines the barycentre of the pion in the transverse plane, and the probability to find it far from $|\mathbf{b}_\perp| = 0$ collapses. On the other hand, when x leaves the neighbourhood of 1, this constraint is released, and as expected, the distribution becomes broader. This is fully consistent with the widening observed when evolving the impact space parameter distribution, since, as highlighted previously, sea quarks and gluons coming from the structure of the dressed quarks carry smaller fractions x of the pion momentum.

These points are more visible on figure 19, which shows the second moment of the distribution in \mathbf{b}_\perp computed as:

$$\langle \mathbf{b}_\perp(x)^2 \rangle = \int d^2\mathbf{b}_\perp \rho^q(x, \mathbf{b}_\perp) \mathbf{b}_\perp^2. \quad (138)$$

Interestingly enough, correlations lead to a significant deviation from a symmetric $\langle \mathbf{b}_\perp(x)^2 \rangle$ distribution with respect to $x \leftrightarrow 1 - x$, emphasising the importance of such correlations in our understanding of hadrons.

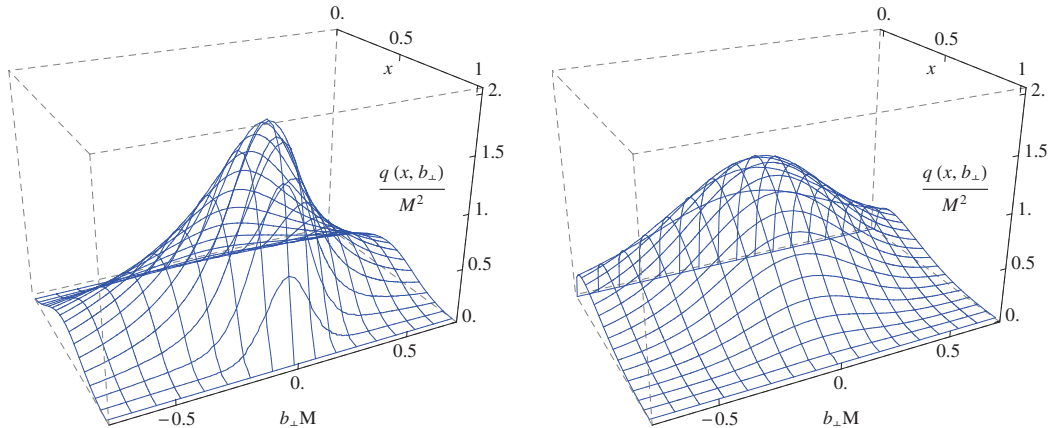


Figure 18: $q(x, \mathbf{b}_\perp)$ using the correlation model of equation (137). Left-hand side: Original scale $\mu_F = 0.51$ GeV. Right-hand side: Final scale at $\mu_F = 2$ GeV.

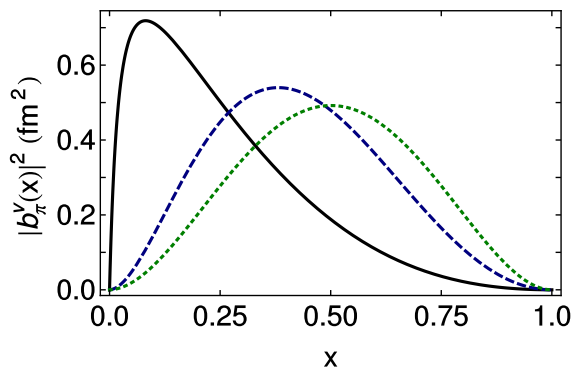


Figure 19: Distribution of the pion's mean-square transverse extend $\langle |\mathbf{b}_\perp(x)|^2 \rangle$ from equation (138) as a function of the longitudinal momentum fraction x . The short-dashed green curve is obtained with $C_\pi^q(x, t) = 1$, the blue long-dashed one with $C_\pi^q(x, t)$ given in equation (137), and the solid line is the evolution of the dashed one from 0.51 GeV to 2 GeV. This figure comes from Ref. [43].

6.3 Strength and weakness of the covariant approach

The covariant modelling of the pion GPD reveals itself to be very encouraging. First, it allows computations in the DSE-BSE framework, due to the use of the Nakanishi representation. Such a representation has been used here to define an algebraic and insightful model of the Bethe-Salpeter amplitude and of the quark propagator. The pion GPDs computed within the algebraic model fulfils the required GPDs theoretical constraints, with the highlighted exception of positivity. However, the comparison with available experimental data is satisfying. It also sheds light on the complications related to the use of a momentum dependent Bethe-Salpeter amplitude. Indeed, the study of the soft pion theorem made here has stressed the importance of the so-called AVWTI, which relates the Bethe-Salpeter amplitude with the quark propagators, constraining the k -dependence of the running quark mass. In the forward case, the absence of the $x \leftrightarrow 1 - x$ symmetry highlights the intrinsic limitations of the impulse approximation in the case of momentum-dependent vertices. Once again, we would like to emphasise that the last two points are somehow invisible for the class of theories using momentum independent vertices, like for instance Nambu-Jona-Lasinio type models [165].

On the other hand, at the time of writing, the restoration of the $x \leftrightarrow 1 - x$ has led to the consideration of additional terms, which expressions are known only in the forward case. This situation make difficult any correct prediction of the ξ -behaviour of the GPDs. These might also be responsible for the restoration of the positivity property. However they have to vanish in the soft pion limit, due to the consistency of the impulse approximation in this case. With no other clues, different strategies must be considered. Among the possibilities, the lightcone formalism provide an alternative way to model GPDs, as explained in the next section.

7 Lightcone formalism

In previous sections, a covariant approach have been followed to model the valence quark GPD, based first on the impulse approximation and including then some additional contributions needed to amend flaws already present in the forward limit. Pinpointing the proper corrections beyond the impulse approximation is a hard task for off-forward kinematics. Therefore, an alternative approach is desirable. In particular, the so-called overlap representation [6, 49, 94, 164] has been invoked in ref. [43] to illustrate the symmetries about the momentum fraction carried by quarks in the two-body problem and provide then with an insightful guide to model its correlations with the momentum transfer. As we will see, if we are provided with a sensible lightcone wave function, the overlap representation opens an avenue to model GPDs, in such a way that the $x \leftrightarrow 1 - x$ symmetry of the forward limit is, by construction, fulfilled. In the following, we highlight how the DSEs allows to compute GPDs using the overlap representation.

7.1 Lightcone wave functions

Before describing GPDs in the lightcone formalism, we start here by reminding the reader some basics about lightcone physics.

7.1.1 Basic facts on lightcone formalism

At a given lightcone time, for instance $z^+ = 0$, let us split the fields $\psi^q(z)$ into a dynamically independent component, usually called the good field and denoted as $\phi^q(z)$, and a so-called “bad” component, which can be deduced from the good one. The good component is a projection of the Dirac field using $\Pi^+ = \frac{1}{2}\gamma^- \gamma^+$. It can be written in terms of a Fourier transform of creation and annihilation operators through:

$$\begin{aligned} \phi^q(z^-, \mathbf{z}_\perp) = \int \frac{dk^+}{k^+} \frac{d^2 \mathbf{k}_\perp}{16\pi^3} \Theta(k^+) \sum_\mu \left[b_q(w) u_+(w) e^{-i(k^+ z^- - \mathbf{k}_\perp \cdot \mathbf{z}_\perp)} \right. \\ \left. + d_q^\dagger(w) v_+(w) e^{i(k^+ z^- - \mathbf{k}_\perp \cdot \mathbf{z}_\perp)} \right], \end{aligned} \quad (139)$$

where μ denotes here the polarisation and $w = (k^+, \mathbf{k}_\perp, \mu)$. The colour indices are omitted for brevity. Θ denotes here the Heaviside function, and u_+ and v_+ are the “good” component of the spinors obtained after projecting using Π^+ . The same procedure can be applied to define the transverse component of the gluon field on the lightcone. The creation and annihilation operators follows the usual anticommutation relations:

$$\begin{aligned} \{b_{q'}(w'), b_q^\dagger(w)\} &= \{d_{q'}(w'), d_q^\dagger(w)\} \\ &= 16\pi^3 k^+ \delta(k'^+ - k^+) \delta^{(2)}(\mathbf{k}'_\perp - \mathbf{k}_\perp) \delta_{\mu'\mu} \delta_{q'q}, \end{aligned} \quad (140)$$

and it is assumed that they act on a trivial perturbative vacuum $|0\rangle$ to generate partonic states:

$$\begin{aligned} |q; w\rangle &= b_q^\dagger(w) |0\rangle, \\ |\bar{q}; w\rangle &= d_q^\dagger(w) |0\rangle. \end{aligned} \quad (141)$$

7.1.2 Hadrons in the lightcone formalism

Then, according to the definitions of the partonic Fock states (141), it is possible to expand a hadron state $|H; P, \lambda\rangle$ of momentum P and polarisation λ on a Fock space of a given number N of partons of quantum numbers generically denoted β , $|N, \beta, k_1 \cdots k_N\rangle$:

$$|H; P, \lambda\rangle = \sum_{N, \beta} \int [dx]_N [d^2\mathbf{k}_\perp]_N \Psi_{N, \beta}^\lambda(\Omega) |N, \beta, k_1 \cdots k_N\rangle, \quad (142)$$

where $\Psi_{N, \beta}^\lambda(\Omega)$ is the N partons lightcone wave function (LCWF), and Ω denotes the set of kinematic variables associated with the considered partons:

$$\Omega = (x_1, \mathbf{k}_{\perp 1}, \cdots, x_N, \mathbf{k}_{\perp N}). \quad (143)$$

The measure terms in equation (142) are given through:

$$[dx]_N = \prod_{i=1}^N dx_i \delta\left(1 - \sum_{i=1}^N x_i\right), \quad (144)$$

$$[d^2\mathbf{k}_\perp]_N = \frac{1}{(16\pi^3)^{N-1}} \prod_{i=1}^N d^2\mathbf{k}_{\perp i} \delta^2\left(\sum_{i=1}^N \mathbf{k}_{\perp i} - \mathbf{P}_\perp\right), \quad (145)$$

and the canonical normalisation of the LCWFs yields:

$$\sum_{N, \beta} \int [dx]_N [d^2\mathbf{k}_\perp]_N |\Psi_{N, \beta}^\lambda(\Omega)|^2 = 1. \quad (146)$$

The lightcone wave functions can be defined in terms of non-local matrix elements. Following Ref. [166], one can introduce the pion wave function with anti parallel quark helicity as:

$$\Psi_{\uparrow\downarrow}(x, \mathbf{k}_\perp) = \frac{1}{2P^+} \int dz^- d\mathbf{z}_\perp e^{ixP^+z^-} e^{-i\mathbf{k}_\perp \mathbf{z}_\perp} \langle 0 | \bar{d}(0) \gamma^+ \gamma^5 u(z) | \pi, P \rangle \Big|_{z^+=0}, \quad (147)$$

and the parallel quark helicity as:

$$ik^i \Psi_{\uparrow\uparrow}(k^+, \mathbf{k}_\perp) = \frac{1}{2P^+} \int dz^- d\mathbf{z}_\perp e^{ik^+z^-} e^{-i\mathbf{k}_\perp \mathbf{z}_\perp} \langle 0 | \bar{d}(0) \sigma^{+i} \gamma_5 u(z) | \pi^+(P) \rangle \Big|_{z^+=0}. \quad (148)$$

These wave functions allow one to write the pion two-body Fock states as:

$$\begin{aligned} |\pi^+, P\rangle_{\uparrow\downarrow}^{2\text{-body}} &= \int \frac{d^2\mathbf{k}_\perp}{(2\pi)^3} \frac{dx}{\sqrt{x(1-x)}} \Psi_{\uparrow\downarrow}(k^+, \mathbf{k}_\perp) \left[b_{u\uparrow}^\dagger(x, \mathbf{k}_\perp) d_{d\downarrow}^\dagger(1-x, -\mathbf{k}_\perp) \right. \\ &\quad \left. + b_{u\downarrow}^\dagger(x, \mathbf{k}_\perp) d_{d\uparrow}^\dagger(1-x, -\mathbf{k}_\perp) \right] |0\rangle, \end{aligned} \quad (149)$$

and:

$$\begin{aligned} |\pi^+, P\rangle_{\uparrow\uparrow}^{2\text{-body}} &= \int \frac{d^2\mathbf{k}_\perp}{(2\pi)^3} \frac{dx}{\sqrt{x(1-x)}} \Psi_{\uparrow\uparrow}(k^+, \mathbf{k}_\perp) \left[(k_1 - ik_2) b_{u\uparrow}^\dagger(x, \mathbf{k}_\perp) d_{d\uparrow}^\dagger(1-x, -\mathbf{k}_\perp) \right. \\ &\quad \left. + (k_1 + ik_2) b_{u\downarrow}^\dagger(x, \mathbf{k}_\perp) d_{d\downarrow}^\dagger(1-x, -\mathbf{k}_\perp) \right] |0\rangle. \end{aligned} \quad (150)$$

7.1.3 Pion lightcone and Bethe-Salpeter wave functions

The goal we pursue here is the derivation of the pion GPD from the pion two-body Fock states requiring the knowledge of the pion two-body lightcone wave functions which can be itself related

to the Bethe-Salpeter wave function introduced in equation 64 by projecting it on the relevant Dirac structure and integrating over k^- :

$$2P^+ \Psi_{\uparrow\downarrow}(k^+, \mathbf{k}_\perp) = \int \frac{dk^-}{2\pi} \text{Tr} [\gamma^+ \gamma_5 \chi(k, P)], \quad (151)$$

$$ik^i 2P^+ \Psi_{\uparrow\uparrow}(k^+, \mathbf{k}_\perp) = \int \frac{dk^-}{2\pi} \text{Tr} [\sigma^{+i} \gamma_5 \chi(k, P)]. \quad (152)$$

Therefore, it is possible to compute the LCWFs, using the algebraic model from equations (79-83), within the same model framework developed with the covariant approach in previous sections. Thus, up to some ambiguities presumably related to the particular choice used for the Nakanishi representation of the Bethe-Salpeter amplitude and to the definition of the vector insertion in the covariant approach, the result we might obtain for the GPD in the forward limit from these LCWFs should be close to the total PDF shown in figure 16.

As the algebraic parameterisation is defined in euclidean space, one of the efficient ways to compute the LCWF is to proceed through the evaluation of the Mellin moments. As the LCWF are \mathbf{k}_\perp -dependent, the 4-vector k is split as $k = q + \mathbf{k}_\perp$, with $q = (q^+, q^-, 0)$. Consequently, the Mellin moments yield:

$$\begin{aligned} \int_0^1 dx x^m \Psi_{\uparrow\downarrow}(x, \mathbf{k}_\perp) &= \int_0^1 dx x^m \int \frac{dq^- dq^+}{(2\pi)^2} \text{Tr} [\gamma^+ \gamma_5 \chi_\pi(q + \mathbf{k}_\perp, P)] \delta(xP \cdot n - q \cdot n) \\ &= \int \frac{d^2 q (q \cdot n)^m}{(2\pi)^2 (P \cdot n)^{(m+1)}} \text{Tr} [\gamma^+ \gamma_5 \chi_\pi(q + \mathbf{k}_\perp, P)]. \end{aligned} \quad (153)$$

Computing the trace and integrating over q using Feynman parameters, one can identify the scalar LCWF as:

$$\Psi_{\uparrow\downarrow}(x, \mathbf{k}_\perp) = -\frac{\Gamma(\nu+1)}{\Gamma(\nu+2)} \frac{M^{2\nu+1} 4^\nu R_\nu}{[\mathbf{k}_\perp^2 + M^2]^{\nu+1}} x^\nu (1-x)^\nu. \quad (154)$$

Using the same approach, the helicity-1 LCWF $\Psi_{\uparrow\uparrow}(k^+, \mathbf{k}_\perp)$ can be computed through its Mellin moments as:

$$\Psi_{\uparrow\uparrow}(x, \mathbf{k}_\perp) = 2iM^{2\nu} \frac{\Gamma(\nu+1)}{\Gamma(\nu+2)} \frac{4^\nu R_\nu x^\nu (1-x)^\nu}{[\mathbf{k}_\perp^2 + M^2]^{\nu+1}} \quad (155)$$

7.2 Overlap of pion wave functions

The equations (154,155) appear to be the main ingredients needed to obtain the valence-quark pion GPD which, as follows, can be derived from the pion Fock states with a two-body truncation.

7.2.1 GPDs and LCWFs

The lightcone formalism is a convenient approach to compute GPDs⁶ [49], since the latter are defined through operators at a given lightcone time. These operators can then be written in terms of good components ϕ of the quark fields ψ :

$$\bar{\psi}^q \left(-\frac{z}{2} \right) \gamma^+ \psi^q \left(\frac{z}{2} \right) \Big|_{z^+=0} = \sqrt{2} \phi_q^\dagger \left(-\frac{z}{2} \right) \phi_q \left(\frac{z}{2} \right). \quad (156)$$

The decomposition of equation (142) leads to the following expression for the pion GPD:

$$\begin{aligned} H(x, \xi, t) &= \sqrt{2} \sum_{N, N'} \sum_{\beta, \beta'} \int [d\hat{x}']_{N'} [d^2 \hat{\mathbf{k}}'_\perp]_{N'} [d\tilde{x}]_N [d^2 \tilde{\mathbf{k}}_\perp]_N \Psi_{N', \beta'}^*(\hat{\Omega}') \Psi_{N, \beta}(\tilde{\Omega}) \\ &\times \int \frac{dz^-}{2\pi} e^{iP^+ z^-} \langle N', \beta, k'_1 \dots k'_N | \phi^{q\dagger} \left(-\frac{z}{2} \right) \phi^q \left(\frac{z}{2} \right) | N, \beta, k_1 \dots k_N \rangle, \end{aligned} \quad (157)$$

⁶We adapt here the derivation of the spin one-half case done in Ref. [49] to the spinless case.

where the hat variables are given in the outgoing pion wave function frame, and the tilde ones in the incoming pion wave function frame. Other variables are considered in the GPD symmetric frame, *i.e.* the frame such that $p_1 = P - \frac{\Delta}{2}$ and $p_2 = P + \frac{\Delta}{2}$. In this latter frame, it is possible to define the average variables \bar{k}_i as:

$$\bar{k}_i = \frac{1}{2}(k_i + k'_i) \quad , \quad \bar{x}_i = \frac{\bar{k}_i^+}{P^+}, \quad (158)$$

which fulfil the momentum conservation sum rules:

$$\sum_{i=1}^N \bar{x}_i = 1 \quad , \quad \sum_{i=1}^N \bar{\mathbf{k}}_{\perp i} = P_{\perp} = 0. \quad (159)$$

Therefore, active parton momentum variables, labelled as j , follow:

$$x_j = \bar{x}_j + \xi \quad , \quad x'_j = \bar{x}_j - \xi \quad , \quad (160)$$

and

$$\mathbf{k}_{\perp j} = \bar{\mathbf{k}}_{\perp j} - \frac{\Delta_{\perp}}{2} \quad , \quad \mathbf{k}'_{\perp j} = \bar{\mathbf{k}}'_{\perp j} + \frac{\Delta_{\perp}}{2} \quad . \quad (161)$$

On the other hands, the other partons variables, labelled i , are simply related through:

$$k'_i = \bar{k}_i = k_i. \quad (162)$$

In the incoming and outgoing momentum frames, one can also define the fraction of momentum \tilde{x}_i and \hat{x}'_i as:

$$\tilde{x}_i = \frac{\tilde{k}_i^+}{p_1^+} \quad , \quad \hat{x}'_i = \frac{\hat{k}'_i}{p_2^+}. \quad (163)$$

It is then possible, to boost these variables from their original frame, to the symmetric frame used here to compute GPDs. Doing so, one gets for the incoming variables:

$$\begin{aligned} \tilde{x}_i &= \frac{\bar{x}_i}{1 + \xi}, & \tilde{\mathbf{k}}_{\perp i} &= \bar{\mathbf{k}}_{\perp i} + \frac{\bar{x}_i}{1 + \xi} \frac{\Delta_{\perp}}{2}, & \text{for } i \neq j \\ \tilde{x}_j &= \frac{\bar{x}_j + \xi}{1 + \xi}, & \tilde{\mathbf{k}}_{\perp j} &= \bar{\mathbf{k}}_{\perp j} - \frac{1 - \bar{x}_j}{1 + \xi} \frac{\Delta_{\perp}}{2}, \end{aligned} \quad (164)$$

and for the outgoing one:

$$\begin{aligned} \hat{x}'_i &= \frac{\bar{x}_i}{1 - \xi}, & \hat{\mathbf{k}}'_{\perp i} &= \bar{\mathbf{k}}_{\perp i} - \frac{\bar{x}_i}{1 - \xi} \frac{\Delta_{\perp}}{2}, & \text{for } i \neq j \\ \hat{x}'_j &= \frac{\bar{x}_j - \xi}{1 - \xi}, & \hat{\mathbf{k}}'_{\perp j} &= \bar{\mathbf{k}}_{\perp j} + \frac{1 - \bar{x}_j}{1 - \xi} \frac{\Delta_{\perp}}{2}. \end{aligned} \quad (165)$$

Denoting now by k the Fourier conjugate of z in equation (157), such as $k^+ = xP^+$, one immediately deduce that $x = \bar{x}_j$. In the case of the pion, equation (157) can be simplify in the DGLAP case to:

$$\begin{aligned} H_{\pi}^q(x, \xi, t)|_{\xi \leq x \leq 1} &= \sum_N \sqrt{1 - \xi}^{2-N} \sqrt{1 + \xi}^{2-N} \sum_{\beta=\beta'} \sum_j \delta_{s_j q} \\ &\times \int [d\bar{x}]_N [d^2 \bar{\mathbf{k}}_{\perp}]_N \delta(x - \bar{x}_j) \Psi_{N,\beta'}^*(\hat{\Omega}') \Psi_{N,\beta}(\tilde{\Omega}). \end{aligned} \quad (166)$$

The ERBL part can be derived similarly to the DGLAP one, but will be non-diagonal in N , as interactions between $\Psi_{N,\beta}(\hat{\Omega})$ and $\Psi_{N+2,\beta}(\tilde{\Omega})$ are expected. Therefore, in the case of a two-body truncation, no ERBL contribution can be computed directly using the lightcone formalism.

However, in the DGLAP case, the two-body truncation yields:

$$\begin{aligned} H_{\pi}^q(x, \xi, t)|_{\xi \leq x \leq 1}^{2\text{-body}} &= \int [d\bar{x}]_2 [d^2 \bar{\mathbf{k}}_{\perp}]_2 \delta(x - \bar{x}_j) \Psi_{\uparrow\downarrow}^*(\hat{\Omega}') \Psi_{\uparrow\downarrow}(\tilde{\Omega}) \\ &+ \int [d\bar{x}]_2 [d^2 \bar{\mathbf{k}}_{\perp}]_2 \delta(x - \bar{x}_j) \left(\hat{k}_1 + i\hat{k}_2 \right) \left(\tilde{k}_1 - i\tilde{k}_2 \right) \Psi_{\uparrow\uparrow}^*(\hat{\Omega}') \Psi_{\uparrow\uparrow}(\tilde{\Omega}). \end{aligned} \quad (167)$$

7.2.2 An example with the algebraic model

It is then possible to inject equations (154) and (155) in equation (167). Introducing the two Feynman parameters u and v and then integrating over \mathbf{k}_\perp , one is left with two contributions coming from the different combinations of the spin of the dressed quarks. Using the fact that, in our euclidean and chiral approach, $t = \frac{\Delta_1^2}{1-\xi^2}$, one gets:

$$H^{\uparrow\downarrow}(x, \xi, t) = \frac{\Gamma(2\nu+2)}{\Gamma(\nu+2)^2} \int du dv u^\nu v^\nu \delta(1-u-v) \frac{(2M^{2\nu} 4^\nu R_\nu)^2 \hat{x}^\nu (1-\hat{x})^\nu \tilde{x}^\nu (1-\tilde{x})^\nu}{\left(t uv \frac{(1-x)^2}{1-\xi^2} + M^2\right)^{2\nu+1}}, \quad (168)$$

and

$$H^{\uparrow\uparrow}(x, \xi, t) = \frac{\Gamma(2\nu+2)}{\Gamma(\nu+2)^2} \int du dv u^\nu v^\nu \delta(1-u-v) (2M^{2\nu} 4^\nu R_\nu)^2 \hat{x}^\nu (1-\hat{x})^\nu \tilde{x}^\nu (1-\tilde{x})^\nu \times \left[\frac{\pi \frac{\Gamma(2\nu)}{\Gamma(2\nu+2)}}{\left(t uv \frac{(1-x)^2}{1-\xi^2} + M^2\right)^{2\nu}} - t \frac{uv \frac{(1-x)^2}{1-\xi^2} \pi \frac{\Gamma(2\nu+1)}{\Gamma(2\nu+2)}}{\left(t uv \frac{(1-x)^2}{1-\xi^2} + M^2\right)^{2\nu+1}} \right]. \quad (169)$$

One can now focus on the case $t = 0$ where the pion quark GPD can be simplified as:

$$H_\pi^q(x, \xi, 0)|_{\text{DGLAP}} = \kappa'_\nu \hat{x}^\nu (1-\hat{x})^\nu \tilde{x}^\nu (1-\tilde{x})^\nu \quad (170)$$

$$= \kappa'_\nu \frac{(1-x)^{2\nu} (x^2 - \xi^2)^\nu}{(1-\xi^2)^{2\nu}}, \quad (171)$$

κ'_ν is therein an overall normalisation constant. In the case $\nu = 1$, $\kappa'_\nu = 30$, and the result of the computation of the GPD in the DGLAP region is illustrated on figure 20.

One can finally deduce, from equation (170), the expression for the PDF computed with the overlap of LCWFs. This is done by taking $\xi = 0$ in addition to $t = 0$ leading to:

$$q_\pi(x) = \kappa'_\nu x^{2\nu} (1-x)^{2\nu}, \quad (172)$$

which should compare well with the PDF obtained in equation (129) within an equivalent framework and a covariant approach based on the impulse approximation and the amendment described in section 6. The comparison is shown by the figure 16, where the agreement between black solid and dotted lines, which correspond to both the total covariant and overlap computations, is striking.

Focusing on figure 20 and the related equation (170), some comments must be made. The first tempting point is of course to compare the overlap results presented in figure 20 with the GPD obtained in the covariant approach through the impulse approximation. The latter result was shown on figure 14. One immediately notices that, the more off-forward, the more different the two DGLAP regions are, although they have been computed from the *very same* Bethe-Salpeter amplitude. The main difference lies in the fact that the overlap computations lead to a GPD which vanishes on the line $x = \xi$, whereas the triangle diagram computation predicts a non-vanishing value of the GPD on this line. As a consequence, the GPD computed in the overlap approach fulfils the positivity property defined in equation (25). When t vanishes, the formulae obtained for the GPD (170) and the PDF (172) lead to a relation stronger than the positivity condition, since:

$$H_\pi^q(x, \xi, 0)|_{\text{DGLAP}} = \sqrt{q_\pi(x_1) q_\pi(x_2)}. \quad (173)$$

This relation between the GPD and the PDF is presumably a feature of the algebraic model defined in equations (79)-(83).

Nevertheless, the fact that the GPD vanishes on the line $x = \xi$ in a two-body approximation is not a surprise, and have been already highlighted in Ref. [112] and Ref. [167] for instance. Moreover, computations using a higher Fock state, including a gluon in addition to the dressed

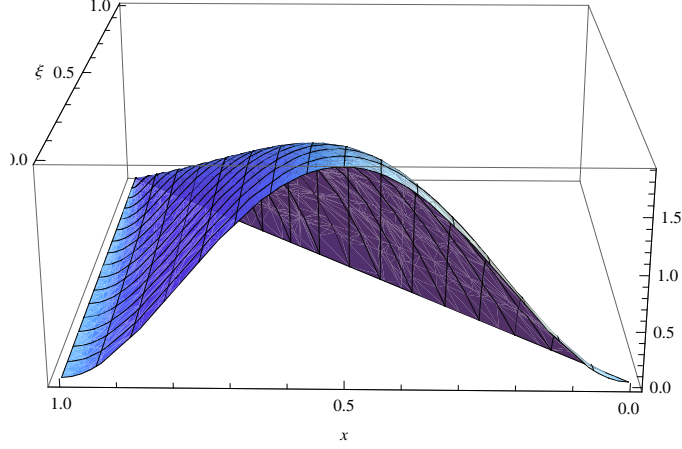


Figure 20: Pion GPD H_π^q as a function of x and ξ obtained through the overlap of LCWFs in the DGLAP region.

quarks, have been performed in Ref. [167]. Using the same computation techniques within this three-body truncation than in two-body truncation, the authors showed that the three-body contribution leads to a non-vanishing GPD on the line $x = \xi$. Therefore, in this kinematic area, the GPD seems to be very sensitive to the truncation of the Fock space. This is of deep phenomenological interest (see section 2.1.4), as the imaginary part of the CFF \mathcal{H} is directly proportional to $H(\xi, \xi, t)$ at leading order.

7.3 Overlap and polynomiality

If the overlap representation offer a simple way to build a GPD model fulfilling the positivity property, the major drawback is that within a two-body truncation, it is not possible to get a proper model for the ERBL region. Therefore, it is a priori impossible to conclude on the polynomiality property of the Mellin moments. However, the fact that the LCWFs are derived from the Bethe-Salpeter wave function suggests that the underlying Lorentz symmetry is preserved. And therefore, one should expect polynomiality to be fulfilled.

The authors of Ref. [168] and Ref. [169] have shown that for a certain class of LCWFs, a simple change of variable allows the identification of the Double Distributions. From the DDs, it is then easy to compute the ERBL part of the GPD through the Radon transform (46). The authors of Ref. [168] use lightcone wave functions such that:

$$\Psi(x, \mathbf{k}_\perp) \propto \frac{M^{2p}}{\sqrt{1-x}} x^{-p} \left(M^2 - \frac{\mathbf{k}_\perp^2 + m^2}{x} - \frac{\mathbf{k}_\perp^2 + \lambda^2}{1-x} \right)^{-p-1}, \quad (174)$$

where M , λ and m are respectively the hadron, the spectator and the quark masses. The associated DD $e(\beta, \alpha, t)$, given in the so-called Pobylitsa scheme [170], for the GPD $E(x, \xi, t)$ is then given by:

$$e(\beta, \alpha, t) = N \frac{\left(\frac{m}{M} + \beta \right) \left((1-\beta)^2 - \alpha^2 \right)^p}{\left[(1-\beta) \frac{m^2}{M^2} + \beta \frac{\lambda^2}{M^2} - \beta(1-\beta) - \left((1-\beta)^2 - \alpha^2 \right) \frac{t}{4M^2} \right]^{2p+1}}, \quad (175)$$

with N an overall normalisation constant. These results show that, even if it not possible to compute directly in the overlap approach a contribution for the ERBL region, it is possible to

deduce one from the DGLAP area. And even more interesting, it is possible to get one which fulfils the polynomiality condition.

Unfortunately, the wave functions of equations (154) and (155) do not belong to the class of functions studied in Ref. [168] and Ref. [169]. Nevertheless, the Radon transform, relating DDs to GPDs, can be inverted. The general inversion formula is given by:

$$f(\beta, \alpha) = \frac{2}{(2\pi)^2} \int_{-\frac{\pi}{2}}^{\frac{\pi}{2}} d\phi \int_{-\infty}^{\infty} d\tau \text{PV} \left[\frac{1}{\tau} \right] \left(\frac{\partial}{\partial s'} \mathcal{R}f(s' + \beta \cos(\phi) + \alpha \sin(\phi) - \tau, \phi) \right) \Big|_{s'=0}, \quad (176)$$

where f is the double distributions, and $\mathcal{R}f$ is its canonical Radon transform. PV stands for the principal value distribution defined as:

$$\int_{-\infty}^{\infty} dx \text{PV} \left[\frac{1}{x} \right] u(x) = \int_0^{\infty} dx \frac{u(x) - u(-x)}{x}. \quad (177)$$

However, as highlighted in Refs. [96, 153], this formula is numerically very sensitive to numerical noise. Moreover, it requires to know the GPDs on an extended support, including the DGLAP and ERBL region, but also the GPDs *alter ego* in terms of crossing symmetry: the Generalised Distribution Amplitudes (GDA) [1, 171, 172]. Therefore, a direct implementation of equation (176) is not suitable for deriving the ERBL contribution from the DGLAP one. However, using the 1CDD scheme defined in equations (55) and (56), one can relate the GPD to the canonical Radon transform $\mathcal{R}f$ of the function f through:

$$\frac{\sqrt{1+\xi^2}}{x} H(x, \xi, t) = \mathcal{R}f = \int_{\Omega} d\beta d\alpha \delta(s - \beta \cos(\phi) - \alpha \sin(\phi)) f(\beta, \alpha, t), \quad (178)$$

with $s = \frac{x}{\cos(\phi)}$ and $\xi = \tan(\phi)$. Then a careful mathematical study of the properties of the Radon transform shows that the double distribution f can be uniquely defined on the entire rhombus, except for the line $\beta = 0$. The proof is left for a forthcoming work [173]. The consequences of these results are important, since one would be able to compute a proper contribution to the GPD in the ERBL region, within a two-body approximation. The deep cause for this comes from the constraints for the GPD imposed by Lorentz and discrete symmetries. The GPDs has to be the Radon transform of a certain DD. In particular, the Radon transform of a 1CDD $f(\beta, \alpha, t)$ can be recast as:

$$\mathcal{R}f(s, \varphi, t) = \sum_{m=0}^{\infty} \sum_{l=0}^m g_{ml}(t) e^{i(-m+2l)\varphi} C_m^{\alpha}(s), \quad (179)$$

where $g_{ml}(t)$ are the coefficients for the expansion in terms of Gegenbauer polynomials, $C_m^{\alpha}(s)$. Therefore, identifying properly the coefficients $g_{ml}(t)$, if possible, leads to the unique extension to the ERBL kinematical region for a GPD only known in the DGLAP domain. However, possible non-analytic contributions would not be visible and might spoil the previous results. The existence of such contributions is still debated [174].

The Radon inversion remains an ill-posed mathematical problem in the sense of Hadamard. In practical, it means that uncertainties like for instance numerical noise, are amplified. Therefore, even if the ERBL region is a priori accessible, the numerical noise might make very hard the path to access it. Nevertheless, this problem may be overcome using proper algorithms. This study is left for a future work [173].

8 Conclusion

Experimental perspectives in hadron physics, and more specifically, in hadron structure will probably challenge our understanding of the non-perturbative sector of the strong interaction. However, without a proper connection of those data with the fundamental theory describing the strong interaction, one will miss a part of the reachable knowledge. In this context, we highlighted the role

that GPDs can play. More precisely, we shed light on the possible achievements in terms of GPD modeling, using non-perturbative techniques such as the Dyson-Schwinger equations. The recent progress in the development of DSE kernels and the use of the Nakanishi representation allow for optimism. Indeed, a two-body effective quark model of a pion GPD, generated dynamically through the DSEs and BSEs, will certainly be a valuable outcome in a very near future. However, such computations must take into account the important features analysed and discussed in the current paper. The algebraic model presented here has highlighted the specific role of the Axial-Vector Ward-Takahashi Identity in the fulfilment of the soft pion theorem. Any dynamical computations should therefore pay a specific attention to this point. In addition, the so-called impulse approximation has been shown beyond any reasonable doubt to be insufficient to ensure the preservation the symmetry related to the fraction of momentum carried by the quarks in the two-body system. If a proper amendment for this flaw resulting from the impulse approximation has been found in the forward case (*i.e.* for the PDF), a piece of the pion GPD is still missing.

However, this problem may be overcome soon through the lightcone formalism. Indeed, recent results suggest that the pion GPDs can be computed after a two-body truncation, both in the DGLAP and ERBL regions. Using a suitable algorithm to compute the inverse Radon transform, it should be possible to obtain the pion GPD in its entire domain of definition. Such a breakthrough would then pave the way for a systematic study of the pion properties, including its 3D shape, in terms of choices of the DSEs kernels.

On a longer time scale, this procedure should of course be extended to the proton, since it will be the main targeted hadron in the forthcoming JLab 12 experiments. Indubitably, the proton case will be significantly more difficult, as one has to deal with a three-body system at the lowest order. However, truncation schemes have also been developed for the Faddeev equations, and a first approximation of the proton in terms of a quark and a diquark may also be relevant. Therefore, it is realistic to consider the possibility of the emergence of DSE-based computations for the proton GPDs in forthcoming years.

Notwithstanding the highlighted challenges, the computation of GPDs within a Dyson-Schwinger framework promises to be an important tool for the interpretation of JLab 12 observables, opening the path to a detailed knowledge on the nucleon structure and a deeper understanding of the large distance regime of the strong interaction.

Acknowledgements

The authors would like to thank L. Chang, C.D. Roberts, F. Sabatié, S.M. Schmidt and P. Tandy with whom parts of the results described here have been derived. They are also grateful to L. Chang, I. Cloet, M. Defurne, J-F. Mathiot, B. Pasquini, B. Pire, C.D. Roberts, F. Sabatié, L. Szymanowski, J. Wagner and S. Wallon for their valuable discussions and comments. The authors are also thankful for the chance to participate in the workshops “Non-Perturbative QCD 2012”, Matalascañas, Spain, where this project originated, “Many Manifestations of Nonperturbative QCD under the Southern Cross”, Ubatuba, Sao Paulo, where significant parts of this work were first presented and improvements discussed, as well as “Non-Perturbative QCD 2014”, Punta Umbria, Spain, where the overlap representation project started being discussed.

This work is partly supported by U.S. Department of Energy, Office of Science, Office of Nuclear Physics, under contract no. DE-AC02-06CH11357, by the Commissariat à l’Energie Atomique, the Joint Research Activity “Study of Strongly Interacting Matter” (acronym HadronPhysics3, Grant Agreement n.283286) under the Seventh Framework Programme of the European Community, by the GDR 3034 PH-QCD “Chromodynamique Quantique et Physique des Hadrons”, the ANR-12-MONU-0008-01 “PARTONS” and the Spanish ministry Research Project FPA2014-53631-C2-2-P.

A Conventions and Notations

A.1 Space-time and lightcone conventions

Four-vectors are denoted with normal character *e.g.* $p = (p^0, p^1, p^2, p^3)$, whereas three- and two-vectors are written in bold font: $\mathbf{p} = (p^1, p^2, p^3)$. The Minkowskian metric used through this text is:

$$\eta_{\mu\nu} = \eta^{\mu\nu} = \begin{pmatrix} 1 & 0 & 0 & 0 \\ 0 & -1 & 0 & 0 \\ 0 & 0 & -1 & 0 \\ 0 & 0 & 0 & -1 \end{pmatrix}, \quad (180)$$

so that:

$$p^2 = (p^0)^2 - \mathbf{p}^2 = M^2. \quad (181)$$

The lightcone variables for a four-vector v are defined as:

$$v^+ = \frac{1}{\sqrt{2}}(v^0 + v^3) \quad , \quad v^- = \frac{1}{\sqrt{2}}(v^0 - v^3) \quad \text{and} \quad \mathbf{v}_\perp = (v^1, v^2). \quad (182)$$

A.2 Dirac Algebra

The Dirac matrices obey the four-dimensional Clifford Algebra:

$$\{\gamma^\mu, \gamma^\nu\} = 2\eta^{\mu\nu}. \quad (183)$$

In all this work, the Weyl representation of the γ^μ is used:

$$\gamma^\mu = \begin{pmatrix} 0 & \bar{\sigma}^\mu \\ \sigma^\mu & 0 \end{pmatrix}, \quad (184)$$

with:

$$\sigma^\mu = (1, \boldsymbol{\sigma}) \quad , \quad \bar{\sigma}^\mu = (1, -\boldsymbol{\sigma}), \quad (185)$$

and the σ^i are the Pauli matrices. The $\sigma^{\mu\nu}$ tensor is defined as:

$$\sigma^{\mu\nu} = \frac{i}{2} [\gamma^\mu, \gamma^\nu]. \quad (186)$$

A.3 Euclidean space

It is usually possible to define a Euclidean quantum field theory which is the counterpart of the Minkowskian one providing that:

$$\int d^4x^M = -i \int d^4x^E, \quad (187)$$

$$\gamma^M \cdot \partial^M = i\gamma^E \cdot \partial^E \quad (188)$$

$$p^M \cdot \gamma^M = -ip^E \cdot \gamma^E \quad (189)$$

$$p^M \cdot q^M = -p^E \cdot q^E, \quad (190)$$

with $x^4 = ix^0$ and $\eta_{\mu\nu}^E = \delta_{\mu\nu}$, $\delta_{\mu\nu}$ being the four dimensional Kronecker symbol. The Euclidean Clifford algebra is given by:

$$\{\gamma_\mu^E, \gamma_\nu^E\} = 2\delta_{\mu\nu}, \quad (191)$$

leading to:

$$\gamma_4^E = \gamma_0^M, \quad \gamma_j^E = -i\gamma_j^M \quad \text{for } j = 1, 2, 3, \quad \gamma_5^E = -\gamma_1^E \gamma_2^E \gamma_3^E \gamma_4^E = \gamma_5^M. \quad (192)$$

We follow these conventions for our computations in Euclidean space.

A.4 Gordon Identity

The Gordon identity relates different Dirac structures through:

$$\bar{u}(p_2)\gamma^\mu u(p_1) = \frac{1}{2M}\bar{u}(p_2)(2P^\mu + i\sigma^{\mu\nu}\Delta_\nu)u(p_1), \quad (193)$$

where M is the mass of the considered hadron and P and Δ are defined as in section 2.

References

- [1] Dieter Mueller, D. Robaschik, B. Geyer, F.M. Dittes, and J. Hořejši. Wave functions, evolution equations and evolution kernels from light ray operators of QCD. *Fortsch.Phys.*, 42:101–141, 1994.
- [2] Xiang-Dong Ji. Deeply virtual Compton scattering. *Phys.Rev.*, D55:7114–7125, 1997.
- [3] A.V. Radyushkin. Nonforward parton distributions. *Phys.Rev.*, D56:5524–5557, 1997.
- [4] Xiang-Dong Ji. Off forward parton distributions. *J.Phys.*, G24:1181–1205, 1998.
- [5] K. Goeke, Maxim V. Polyakov, and M. Vanderhaeghen. Hard exclusive reactions and the structure of hadrons. *Prog.Part.Nucl.Phys.*, 47:401–515, 2001.
- [6] M. Diehl. Generalized parton distributions. *Phys.Rept.*, 388:41–277, 2003.
- [7] A.V. Belitsky and A.V. Radyushkin. Unraveling hadron structure with generalized parton distributions. *Phys.Rept.*, 418:1–387, 2005.
- [8] Sigfrido Boffi and Barbara Pasquini. Generalized parton distributions and the structure of the nucleon. *Riv.Nuovo Cim.*, 30:387, 2007.
- [9] Michel Guidal, Hervé Moutarde, and Marc Vanderhaeghen. Generalized Parton Distributions in the valence region from Deeply Virtual Compton Scattering. *Rept.Prog.Phys.*, 76:066202, 2013.
- [10] M. Defurne, M. Amarian, K.A. Aniol, M. Beaumel, H. Benaoum, et al. The E00-110 experiment in Jefferson Lab’s Hall A: Deeply Virtual Compton Scattering off the Proton at 6 GeV. 2015.
- [11] H.S. Jo et al. Cross sections for the exclusive photon electroproduction on the proton and Generalized Parton Distributions. 2015.
- [12] Andrzej Sandacz. The GPD program at COMPASS. In *12th Conference on the Intersections of Particle and Nuclear Physics (CIPANP 2015) Vail, Colorado, USA, May 19-24, 2015*, 2015.
- [13] A. Accardi, J.L. Albacete, M. Anselmino, N. Armesto, E.C. Aschenauer, et al. Electron Ion Collider: The Next QCD Frontier - Understanding the glue that binds us all. 2012.
- [14] V.M. Braun, A.N. Manashov, and B. Pirnay. Finite- t and target mass corrections to DVCS on a scalar target. *Phys.Rev.*, D86:014003, 2012.
- [15] V.M. Braun, A.N. Manashov, and B. Pirnay. Finite- t and target mass corrections to deeply virtual Compton scattering. *Phys.Rev.Lett.*, 109:242001, 2012.
- [16] M. Guidal, M.V. Polyakov, A.V. Radyushkin, and M. Vanderhaeghen. Nucleon form-factors from generalized parton distributions. *Phys.Rev.*, D72:054013, 2005.
- [17] S.V. Goloskokov and P. Kroll. Vector meson electroproduction at small Bjorken- x and generalized parton distributions. *Eur.Phys.J.*, C42:281–301, 2005.

- [18] Maxim V. Polyakov and Kirill M. Semenov-Tian-Shansky. Dual parametrization of GPDs versus double distribution Ansatz. *Eur.Phys.J.*, A40:181–198, 2009.
- [19] Kresimir Kumerički and Dieter Mueller. Deeply virtual Compton scattering at small x_B and the access to the GPD H. *Nucl.Phys.*, B841:1–58, 2010.
- [20] Gary R. Goldstein, J. Osvaldo Gonzalez Hernandez, and Simonetta Liuti. Flexible Parametrization of Generalized Parton Distributions from Deeply Virtual Compton Scattering Observables. *Phys.Rev.*, D84:034007, 2011.
- [21] Maxim V. Polyakov and C. Weiss. Skewed and double distributions in pion and nucleon. *Phys.Rev.*, D60:114017, 1999.
- [22] I.V. Anikin, A.E. Dorokhov, A.E. Maximov, L. Tomio, and V. Vento. Off diagonal quark distribution functions of the pion within an effective single instanton approximation. 1999.
- [23] Wojciech Broniowski and Enrique Ruiz Arriola. Impact parameter dependence of the generalized parton distribution of the pion in chiral quark models. *Phys.Lett.*, B574:57–64, 2003.
- [24] Wojciech Broniowski, Enrique Ruiz Arriola, and Krzysztof Golec-Biernat. Generalized parton distributions of the pion in chiral quark models and their QCD evolution. *Phys.Rev.*, D77:034023, 2008.
- [25] Alexander E. Dorokhov, Wojciech Broniowski, and Enrique Ruiz Arriola. Generalized Quark Transversity Distribution of the Pion in Chiral Quark Models. *Phys.Rev.*, D84:074015, 2011.
- [26] F.J. Dyson. The S matrix in quantum electrodynamics. *Phys.Rev.*, 75:1736–1755, 1949.
- [27] Julian S. Schwinger. On the Green’s functions of quantized fields. 1. *Proc.Nat.Acad.Sci.*, 37:452–455, 1951.
- [28] Julian S. Schwinger. On the Green’s functions of quantized fields. 2. *Proc.Nat.Acad.Sci.*, 37:455–459, 1951.
- [29] E.E. Salpeter and H.A. Bethe. A Relativistic equation for bound state problems. *Phys.Rev.*, 84:1232–1242, 1951.
- [30] Murray Gell-Mann and Francis Low. Bound states in quantum field theory. *Phys.Rev.*, 84:350–354, 1951.
- [31] Julian S. Schwinger. The Theory of quantized fields. 2. *Phys.Rev.*, 91:713–728, 1953.
- [32] Lei Chang and Craig D. Roberts. Sketching the Bethe-Salpeter kernel. *Phys.Rev.Lett.*, 103:081601, 2009.
- [33] Lei Chang and Craig D. Roberts. Tracing masses of ground-state light-quark mesons. *Phys.Rev.*, C85:052201, 2012.
- [34] H.L.L. Roberts, A. Bashir, L.X. Gutierrez-Guerrero, C.D. Roberts, and D.J. Wilson. pi- and rho-mesons, and their diquark partners, from a contact interaction. *Phys.Rev.*, C83:065206, 2011.
- [35] B.C. Tiburzi and G.A. Miller. Generalized parton distributions and double distributions for q anti-q pions. *Phys.Rev.*, D67:113004, 2003.
- [36] L. Theussl, S. Noguera, and V. Vento. Generalized parton distributions of the pion in a Bethe-Salpeter approach. *Eur.Phys.J.*, A20:483–498, 2004.
- [37] F. Bissey, J.R. Cudell, J. Cugnon, J.P. Lansberg, and P. Stassart. A Model for the off forward structure functions of the pion. *Phys.Lett.*, B587:189–200, 2004.

- [38] A. Van Dyck, T. Van Cauteren, and Jan Ryckebusch. Support of generalized parton distributions in Bethe-Salpeter models of hadrons. *Phys.Lett.*, B662:413–416, 2008.
- [39] T. Frederico, E. Pace, B. Pasquini, and G. Salme. Pion Generalized Parton Distributions with covariant and Light-front constituent quark models. *Phys.Rev.*, D80:054021, 2009.
- [40] Lei Chang, I.C. Cloet, J.J. Cobos-Martinez, C.D. Roberts, S.M. Schmidt, et al. Imaging dynamical chiral symmetry breaking: pion wave function on the light front. *Phys.Rev.Lett.*, 110:132001, 2013.
- [41] Lei Chang, Cédric Mezrag, Hervé Moutarde, Craig D. Roberts, Jose Rodriguez-Quintero, et al. Basic features of the pion valence-quark distribution function. *Phys.Lett.*, B737:23–29, 2014.
- [42] C. Mezrag, H. Moutarde, J. Rodríguez-Quintero, and F. Sabatié. Towards a Pion Generalized Parton Distribution Model from Dyson-Schwinger Equations. 2014.
- [43] C. Mezrag, L. Chang, H. Moutarde, C.D. Roberts, J. Rodríguez-Quintero, et al. Sketching the pion’s valence-quark generalised parton distribution. *Phys.Lett.*, B741:190–196, 2014.
- [44] Pieter Maris and Craig D. Roberts. Dyson-Schwinger equations: A Tool for hadron physics. *Int.J.Mod.Phys.*, E12:297–365, 2003.
- [45] Ian C. Cloet and Craig D. Roberts. Explanation and Prediction of Observables using Continuum Strong QCD. *Prog.Part.Nucl.Phys.*, 77:1–69, 2014.
- [46] M. Diehl. Generalized parton distributions with helicity flip. *Eur. Phys. J.*, C19:485–492, 2001.
- [47] Markus Diehl and Thierry Gousset. Time ordering in off diagonal parton distributions. *Phys.Lett.*, B428:359–370, 1998.
- [48] Maxim V. Polyakov. Hard exclusive electroproduction of two pions and their resonances. *Nucl.Phys.*, B555:231, 1999.
- [49] M. Diehl, T. Feldmann, R. Jakob, and P. Kroll. The Overlap representation of skewed quark and gluon distributions. *Nucl.Phys.*, B596:33–65, 2001.
- [50] B. Pire, Jacques Soffer, and O. Teryaev. Positivity constraints for off - forward parton distributions. *Eur.Phys.J.*, C8:103–106, 1999.
- [51] P.V. Pobylitsa. Inequalities for generalized parton distributions H and E. *Phys.Rev.*, D65:077504, 2002.
- [52] P.V. Pobylitsa. Disentangling positivity constraints for generalized parton distributions. *Phys.Rev.*, D65:114015, 2002.
- [53] M. Diehl. Generalized parton distributions in impact parameter space. *Eur.Phys.J.*, C25:223–232, 2002.
- [54] Kenneth G. Wilson. Nonlagrangian models of current algebra. *Phys.Rev.*, 179:1499–1512, 1969.
- [55] S.A. Anikin and O.I. Zavyalov. Short Distance and Light Cone Expansions for Products of Currents. *Annals Phys.*, 116:135–166, 1978.
- [56] John C. Collins, Leonid Frankfurt, and Mark Strikman. Factorization for hard exclusive electroproduction of mesons in QCD. *Phys.Rev.*, D56:2982–3006, 1997.
- [57] Xiang-Dong Ji and Jonathan Osborne. One loop corrections and all order factorization in deeply virtual Compton scattering. *Phys.Rev.*, D58:094018, 1998.

- [58] John C. Collins and Andreas Freund. Proof of factorization for deeply virtual Compton scattering in QCD. *Phys.Rev.*, D59:074009, 1999.
- [59] A.V. Radyushkin. Scaling limit of deeply virtual Compton scattering. *Phys.Lett.*, B380:417–425, 1996.
- [60] F.X. Girod et al. Measurement of Deeply virtual Compton scattering beam-spin asymmetries. *Phys.Rev.Lett.*, 100:162002, 2008.
- [61] Morgan J. Murray. Physics Updates from HERMES. *AIP Conf.Proc.*, 1523:46–50, 2012.
- [62] S. Chekanov et al. Measurement of deeply virtual Compton scattering at HERA. *Phys.Lett.*, B573:46–62, 2003.
- [63] A. Aktas et al. Measurement of deeply virtual compton scattering at HERA. *Eur. Phys. J.*, C44:1–11, 2005.
- [64] M. Guidal. A Fitter code for Deep Virtual Compton Scattering and Generalized Parton Distributions. *Eur.Phys.J.*, A37:319–332, 2008.
- [65] H. Moutarde. Extraction of the Compton Form Factor H from DVCS measurements at Jefferson Lab. *Phys.Rev.*, D79:094021, 2009.
- [66] Kresimir Kumerički, Dieter Müller, and Morgan Murray. Revealing CFFs and GPDs from experimental measurements. *Nuovo Cim.*, C036(05):159–165, 2013.
- [67] Kresimir Kumericki, Dieter Mueller, and Andreas Schafer. Neural network generated parametrizations of deeply virtual Compton form factors. *JHEP*, 1107:073, 2011.
- [68] Xiang-Dong Ji and Jonathan Osborne. One loop QCD corrections to deeply virtual Compton scattering: The Parton helicity independent case. *Phys.Rev.*, D57:1337–1340, 1998.
- [69] L. Mankiewicz, G. Piller, E. Stein, M. Vanttinen, and T. Weigl. NLO corrections to deeply virtual Compton scattering. *Phys.Lett.*, B425:186–192, 1998.
- [70] Andrei V. Belitsky, Dieter Mueller, L. Niedermeier, and A. Schafer. Deeply virtual Compton scattering in next-to-leading order. *Phys.Lett.*, B474:163–169, 2000.
- [71] Andreas Freund and Martin McDermott. A Detailed next-to-leading order QCD analysis of deeply virtual Compton scattering observables. *Eur.Phys.J.*, C23:651–674, 2002.
- [72] A. Freund and M.F. McDermott. A Next-to-leading order analysis of deeply virtual Compton scattering. *Phys.Rev.*, D65:091901, 2002.
- [73] Andreas Freund and Martin F. McDermott. A Next-to-leading order QCD analysis of deeply virtual Compton scattering amplitudes. *Phys.Rev.*, D65:074008, 2002.
- [74] B. Pire, L. Szymanowski, and J. Wagner. NLO corrections to timelike, spacelike and double deeply virtual Compton scattering. *Phys.Rev.*, D83:034009, 2011.
- [75] H. Moutarde, B. Pire, F. Sabatie, L. Szymanowski, and J. Wagner. On timelike and spacelike deeply virtual Compton scattering at next to leading order. *Phys.Rev.*, D87:054029, 2013.
- [76] B. Geyer, D. Robaschik, Michael Bordag, and J. Horejsi. NONLOCAL LIGHT CONE EXPANSIONS AND EVOLUTION EQUATIONS. *Z.Phys.*, C26:591–600, 1985.
- [77] T. Braunschweig, B. Geyer, J. Horejsi, and D. Robaschik. Hadron Operators on the Light Cone. *Z.Phys.*, C33:275, 1986.

- [78] F.M. Dittes, Dieter Mueller, D. Robaschik, B. Geyer, and J. Horejsi. The Altarelli-Parisi Kernel as Asymptotic Limit of an Extended Brodsky-Lepage Kernel. *Phys.Lett.*, B209:325–329, 1988.
- [79] I.I. Balitsky and A.V. Radyushkin. Light ray evolution equations and leading twist parton helicity dependent nonforward distributions. *Phys.Lett.*, B413:114–121, 1997.
- [80] A.V. Radyushkin. Double distributions and evolution equations. *Phys.Rev.*, D59:014030, 1999.
- [81] Johannes Blumlein, Bodo Geyer, and Dieter Robaschik. On the evolution kernels of twist-2 light ray operators for unpolarized and polarized deep inelastic scattering. *Phys.Lett.*, B406:161–170, 1997.
- [82] Johannes Blumlein, Bodo Geyer, and Dieter Robaschik. The Virtual Compton amplitude in the generalized Bjorken region: twist-2 contributions. *Nucl.Phys.*, B560:283–344, 1999.
- [83] Andrei V. Belitsky and Dieter Mueller. Next-to-leading order evolution of twist-2 conformal operators: The Abelian case. *Nucl.Phys.*, B527:207–234, 1998.
- [84] Andrei V. Belitsky and Dieter Mueller. Broken conformal invariance and spectrum of anomalous dimensions in QCD. *Nucl.Phys.*, B537:397–442, 1999.
- [85] Andrei V. Belitsky, Dieter Mueller, and A. Freund. Reconstruction of nonforward evolution kernels. *Phys.Lett.*, B461:270–279, 1999.
- [86] Andrei V. Belitsky and Dieter Mueller. Exclusive evolution kernels in two loop order: Parity even sector. *Phys.Lett.*, B464:249–256, 1999.
- [87] Andrei V. Belitsky, A. Freund, and Dieter Mueller. Evolution kernels of skewed parton distributions: Method and two loop results. *Nucl.Phys.*, B574:347–406, 2000.
- [88] A.V. Efremov and A.V. Radyushkin. Asymptotical Behavior of Pion Electromagnetic Form-Factor in QCD. *Theor.Math.Phys.*, 42:97–110, 1980.
- [89] V.L. Chernyak, A.R. Zhitnitsky, and V.G. Serbo. Asymptotic hadronic form-factors in quantum chromodynamics. *JETP Lett.*, 26:594–597, 1977.
- [90] Glennys R. Farrar and Darrell R. Jackson. The Pion Form-Factor. *Phys.Rev.Lett.*, 43:246, 1979.
- [91] G. Peter Lepage and Stanley J. Brodsky. Exclusive Processes in Quantum Chromodynamics: Evolution Equations for Hadronic Wave Functions and the Form-Factors of Mesons. *Phys.Lett.*, B87:359–365, 1979.
- [92] G. Peter Lepage and Stanley J. Brodsky. Exclusive Processes in Perturbative Quantum Chromodynamics. *Phys.Rev.*, D22:2157, 1980.
- [93] A.V. Vinnikov. Code for prompt numerical computation of the leading order GPD evolution. 2006.
- [94] Matthias Burkardt. Impact parameter dependent parton distributions and off forward parton distributions for $\zeta \rightarrow 0$. *Phys. Rev.*, D62:071503, 2000. [Erratum: *Phys. Rev.* D66,119903(2002)].
- [95] A.V. Radyushkin. Asymmetric gluon distributions and hard diffractive electroproduction. *Phys.Lett.*, B385:333–342, 1996.
- [96] O.V. Teryaev. Crossing and radon tomography for generalized parton distributions. *Phys.Lett.*, B510:125–132, 2001.

- [97] B.C. Tiburzi. Double distributions: Loose ends. *Phys.Rev.*, D70:057504, 2004.
- [98] Andrei V. Belitsky, Dieter Mueller, A. Kirchner, and A. Schafer. Twist three analysis of photon electroproduction off pion. *Phys.Rev.*, D64:116002, 2001.
- [99] S.V. Goloskokov and P. Kroll. The Role of the quark and gluon GPDs in hard vector-meson electroproduction. *Eur.Phys.J.*, C53:367–384, 2008.
- [100] S.V. Goloskokov and P. Kroll. An Attempt to understand exclusive π^+ electroproduction. *Eur.Phys.J.*, C65:137–151, 2010.
- [101] C. Mezrag, H. Moutarde, and F. Sabatié. Test of two new parameterizations of the Generalized Parton Distribution H . *Phys.Rev.*, D88:014001, 2013.
- [102] M. Vanderhaeghen, Pierre A.M. Guichon, and M. Guidal. Hard electroproduction of photons and mesons on the nucleon. *Phys.Rev.Lett.*, 80:5064–5067, 1998.
- [103] Pierre A.M. Guichon and M. Vanderhaeghen. Virtual Compton scattering off the nucleon. *Prog.Part.Nucl.Phys.*, 41:125–190, 1998.
- [104] M. Vanderhaeghen, Pierre A.M. Guichon, and M. Guidal. Deeply virtual electroproduction of photons and mesons on the nucleon: Leading order amplitudes and power corrections. *Phys.Rev.*, D60:094017, 1999.
- [105] Peter Kroll, Herve Moutarde, and Franck Sabatie. From hard exclusive meson electroproduction to deeply virtual Compton scattering. *Eur.Phys.J.*, C73:2278, 2013.
- [106] M.V. Polyakov and A.G. Shuvaev. On’dual’ parametrizations of generalized parton distributions. 2002.
- [107] Dieter Müller, Maxim V. Polyakov, and Kirill M. Semenov-Tian-Shansky. Dual parametrization of generalized parton distributions in two equivalent representations. *JHEP*, 1503:052, 2015.
- [108] Dieter Mueller and A. Schafer. Complex conformal spin partial wave expansion of generalized parton distributions and distribution amplitudes. *Nucl.Phys.*, B739:1–59, 2006.
- [109] E. Ruiz Arriola. Pion structure at high-energies and low-energies in chiral quark models. *Acta Phys.Polon.*, B33:4443–4479, 2002.
- [110] Chr.V. Christov, A. Blotz, Hyun-Chul Kim, P. Pobylitsa, T. Watabe, et al. Baryons as nontopological chiral solitons. *Prog.Part.Nucl.Phys.*, 37:91–191, 1996.
- [111] Ho-Meoyng Choi, Chueng-Ryong Ji, and L.S. Kisslinger. Skewed quark distribution of the pion in the light front quark model. *Phys.Rev.*, D64:093006, 2001.
- [112] Ho-Meoyng Choi, Chueng-Ryong Ji, and L.S. Kisslinger. Continuity of skewed parton distributions for the pion virtual Compton scattering. *Phys.Rev.*, D66:053011, 2002.
- [113] A. Mukherjee, I.V. Musatov, H.C. Pauli, and A.V. Radyushkin. Power law wave functions and generalized parton distributions for pion. *Phys.Rev.*, D67:073014, 2003.
- [114] Alexander P. Bakulev, Rusko Ruskov, Klaus Goeke, and N.G. Stefanis. Parton skewed distributions in the pion and quark - hadron duality. *Phys.Rev.*, D62:054018, 2000.
- [115] C. Vogt. The Skewed quark distribution of the pion at large momentum transfer. *Phys.Rev.*, D64:057501, 2001.
- [116] Pervez Hoodbhoy, Xiang-dong Ji, and Feng Yuan. Probing quark distribution amplitudes through generalized parton distributions at large momentum transfer. *Phys.Rev.Lett.*, 92:012003, 2004.

- [117] Daniela Amrath, Markus Diehl, and Jean-Philippe Lansberg. Deeply virtual Compton scattering on a virtual pion target. *Eur.Phys.J.*, C58:179–192, 2008.
- [118] I.V. Musatov and A.V. Radyushkin. Evolution and models for skewed parton distributions. *Phys.Rev.*, D61:074027, 2000.
- [119] M. Diehl, A. Manashov, and A. Schafer. Generalized parton distributions for the pion in chiral perturbation theory. *Phys.Lett.*, B622:69–82, 2005.
- [120] R.F. Streater and A.S. Wightman. *PCT, spin and statistics, and all that*. W.A. Benjamin Inc, 1980.
- [121] E. Seiler. *Gauge Theories as a problem of Constructive Quantum Field Theory and Statistical Mechanics*. Springer-Verlag, 1982.
- [122] J. Glimm and Arthur M. Jaffe. *QUANTUM PHYSICS. A FUNCTIONAL INTEGRAL POINT OF VIEW*. Springer-Verlag, 1987.
- [123] Adnan Bashir, Lei Chang, Ian C. Cloet, Bruno El-Bennich, Yu-Xin Liu, et al. Collective perspective on advances in Dyson-Schwinger Equation QCD. *Commun.Theor.Phys.*, 58:79–134, 2012.
- [124] Gernot Eichmann. From quarks and gluons to baryon form factors. *Prog. Part. Nucl. Phys.*, 67:234–238, 2012.
- [125] H.J. Munczek. Dynamical chiral symmetry breaking, Goldstone’s theorem and the consistency of the Schwinger-Dyson and Bethe-Salpeter Equations. *Phys.Rev.*, D52:4736–4740, 1995.
- [126] A. Bender, Craig D. Roberts, and L. Von Smekal. Goldstone theorem and diquark confinement beyond rainbow ladder approximation. *Phys.Lett.*, B380:7–12, 1996.
- [127] Si-xue Qin, Lei Chang, Yu-xin Liu, Craig D. Roberts, and David J. Wilson. Interaction model for the gap equation. *Phys.Rev.*, C84:042202, 2011.
- [128] Si-xue Qin, Lei Chang, Yu-xin Liu, Craig D. Roberts, and David J. Wilson. Investigation of rainbow-ladder truncation for excited and exotic mesons. *Phys. Rev.*, C85:035202, 2012.
- [129] A. Holl, A. Krassnigg, P. Maris, C.D. Roberts, and S.V. Wright. Electromagnetic properties of ground and excited state pseudoscalar mesons. *Phys.Rev.*, C71:065204, 2005.
- [130] M.S. Bhagwat, M.A. Pichowsky, C.D. Roberts, and P.C. Tandy. Analysis of a quenched lattice QCD dressed quark propagator. *Phys.Rev.*, C68:015203, 2003.
- [131] M.S. Bhagwat and P.C. Tandy. Analysis of full-QCD and quenched-QCD lattice propagators. *AIP Conf.Proc.*, 842:225–227, 2006.
- [132] Patrick O. Bowman, Urs M. Heller, Derek B. Leinweber, Maria B. Parappilly, Anthony G. Williams, et al. Unquenched quark propagator in Landau gauge. *Phys.Rev.*, D71:054507, 2005.
- [133] C.H. Llewellyn-Smith. A relativistic formulation for the quark model for mesons. *Annals Phys.*, 53:521–558, 1969.
- [134] D. Lurié, A. J. Macfarlane, and Y. Takahashi. Normalization of bethe-salpeter wave functions. *Phys. Rev.*, 140:B1091–B1099, Nov 1965.
- [135] Pieter Maris and Peter C. Tandy. Bethe-Salpeter study of vector meson masses and decay constants. *Phys.Rev.*, C60:055214, 1999.

- [136] Pieter Maris, Craig D. Roberts, and Peter C. Tandy. Pion mass and decay constant. *Phys.Lett.*, B420:267–273, 1998.
- [137] Axel Bender, William Detmold, C.D. Roberts, and Anthony William Thomas. Bethe-Salpeter equation and a nonperturbative quark gluon vertex. *Phys.Rev.*, C65:065203, 2002.
- [138] Lei Chang, Craig D. Roberts, and Sebastian M. Schmidt. Dressed-quarks and the nucleon’s axial charge. *Phys.Rev.*, C87:015203, 2013.
- [139] Pieter Maris and Craig D. Roberts. Pseudovector components of the pion, $\pi^0 \rightarrow \gamma \gamma$, and $F(\pi) (q^2)$. *Phys.Rev.*, C58:3659–3665, 1998.
- [140] James S. Ball and Ting-Wai Chiu. Analytic Properties of the Vertex Function in Gauge Theories. 1. *Phys.Rev.*, D22:2542, 1980.
- [141] Chen Chen, Lei Chang, Craig D. Roberts, Shaolong Wan, and David J. Wilson. Spectrum of hadrons with strangeness. *Few Body Syst.*, 53:293–326, 2012.
- [142] Daniele Binosi, Lei Chang, Joannis Papavassiliou, and Craig D. Roberts. Bridging a gap between continuum-QCD and ab initio predictions of hadron observables. *Phys. Lett.*, B742:183–188, 2015.
- [143] A. Bashir, A. Raya, I.C. Cloet, and C.D. Roberts. Regarding confinement and dynamical chiral symmetry breaking in QED3. *Phys.Rev.*, C78:055201, 2008.
- [144] K. Raya, A. Bashir, S. Hernández-Ortiz, A. Raya, and C. D. Roberts. Multiple solutions for the fermion mass function in QED3. *Phys. Rev.*, D88(9):096003, 2013.
- [145] Noboru Nakanishi. Partial-Wave Bethe-Salpeter Equation. *Phys.Rev.*, 130:1230–1235, 1963.
- [146] V.A. Karmanov and J. Carbonell. Solving Bethe-Salpeter equation in Minkowski space. *Eur.Phys.J.*, A27:1–9, 2006.
- [147] Chao Shi, Chen Chen, Lei Chang, Craig D. Roberts, Sebastian M. Schmidt, and Hong-Shi Zong. Kaon and pion parton distribution amplitudes to twist-three. *Phys. Rev.*, D92:014035, 2015.
- [148] Minghui Ding, Fei Gao, Lei Chang, Yu-Xin Liu, and Craig D. Roberts. Leading-twist parton distribution amplitudes of S-wave heavy-quarkonia. 2015.
- [149] B. Z. Kopeliovich, Iván Schmidt, and M. Siddikov. Nonperturbative features of the axial current. *Nucl. Phys.*, A918:41–60, 2013.
- [150] S. Mandelstam. Dynamical variables in the Bethe-Salpeter formalism. *Proc.Roy.Soc.Lond.*, A233:248, 1955.
- [151] K. Nishijima and A. H. Singh. Normalization of bethe-salpeter amplitudes. *Phys. Rev.*, 162:1740–1746, Oct 1967.
- [152] Matthias Aicher, Andreas Schafer, and Werner Vogelsang. Soft-gluon resummation and the valence parton distribution function of the pion. *Phys.Rev.Lett.*, 105:252003, 2010.
- [153] Cedric Mezrag. *Generalised Parton Distributions : from phenomenological approaches to Dyson-Schwinger equations*. PhD thesis, IRFU, SPhN, Saclay, 2015.
- [154] S.R. Amendolia et al. A Measurement of the Space - Like Pion Electromagnetic Form-Factor. *Nucl.Phys.*, B277:168, 1986.
- [155] G.M. Huber et al. Charged pion form-factor between $Q^2 = 0.60\text{-GeV}^2$ and 2.45-GeV^2 . II. Determination of, and results for, the pion form-factor. *Phys.Rev.*, C78:045203, 2008.

- [156] M.L. Goldberger and S.B. Treiman. Form-factors in Beta decay and muon capture. *Phys.Rev.*, 111:354–361, 1958.
- [157] L. Chang, C. Mezrag, H. Moutarde, C.D. Roberts, J. Rodríguez-Quintero, et al. DSE inspired model for the pion’s valence dressed-quark GPD. 2015.
- [158] Z.F. Ezawa. Wide-Angle Scattering in Softened Field Theory. *Nuovo Cim.*, A23:271–290, 1974.
- [159] Glennys R. Farrar and Darrell R. Jackson. Pion and Nucleon Structure Functions Near $x=1$. *Phys.Rev.Lett.*, 35:1416, 1975.
- [160] Stanley J. Brodsky, Matthias Burkardt, and Ivan Schmidt. Perturbative QCD constraints on the shape of polarized quark and gluon distributions. *Nucl.Phys.*, B441:197–214, 1995.
- [161] Xiang-dong Ji, Jian-Ping Ma, and Feng Yuan. Factorization of large- x quark distributions in a hadron. *Phys.Lett.*, B610:247–252, 2005.
- [162] Jacques C.R. Bloch, Craig D. Roberts, and S.M. Schmidt. Selected nucleon form-factors and a composite scalar diquark. *Phys.Rev.*, C61:065207, 2000.
- [163] M.B. Hecht, Craig D. Roberts, and S.M. Schmidt. Valence quark distributions in the pion. *Phys.Rev.*, C63:025213, 2001.
- [164] Matthias Burkardt. Impact parameter space interpretation for generalized parton distributions. *Int. J. Mod. Phys.*, A18:173–208, 2003.
- [165] Yoichiro Nambu and G. Jona-Lasinio. Dynamical Model of Elementary Particles Based on an Analogy with Superconductivity. 1. *Phys. Rev.*, 122:345–358, 1961.
- [166] Matthias Burkardt, Xiang-dong Ji, and Feng Yuan. Scale dependence of hadronic wave functions and parton densities. *Phys. Lett.*, B545:345–351, 2002.
- [167] Chueng-Ryong Ji, Yuriy Mishchenko, and Anatoly Radyushkin. Higher Fock state contributions to the generalized parton distribution of pion. *Phys.Rev.*, D73:114013, 2006.
- [168] D.S. Hwang and Dieter Mueller. Implication of the overlap representation for modelling generalized parton distributions. *Phys.Lett.*, B660:350–359, 2008.
- [169] Dieter Müller and Dae Sung Hwang. The concept of phenomenological light-front wave functions – Regge improved diquark model predictions. 2014.
- [170] P.V. Pobylitsa. Solution of polynomiality and positivity constraints on generalized parton distributions. *Phys.Rev.*, D67:034009, 2003.
- [171] M. Diehl, T. Gousset, B. Pire, and O. Teryaev. Probing partonic structure in $\gamma^* \gamma \rightarrow \pi \pi$ near threshold. *Phys.Rev.Lett.*, 81:1782–1785, 1998.
- [172] M. Diehl, T. Gousset, and B. Pire. Exclusive production of pion pairs in $\gamma^* \gamma$ collisions at large Q^2 . *Phys.Rev.*, D62:073014, 2000.
- [173] C. Mezrag, H. Moutarde, and J. Rodríguez-Quintero. Forthcoming paper on radon transform. 2016.
- [174] Dieter Müller and Kirill M. Semenov-Tian-Shansky. $J = 0$ fixed pole and D -term form factor in deeply virtual Compton scattering. *Phys. Rev.*, D92(7):074025, 2015.